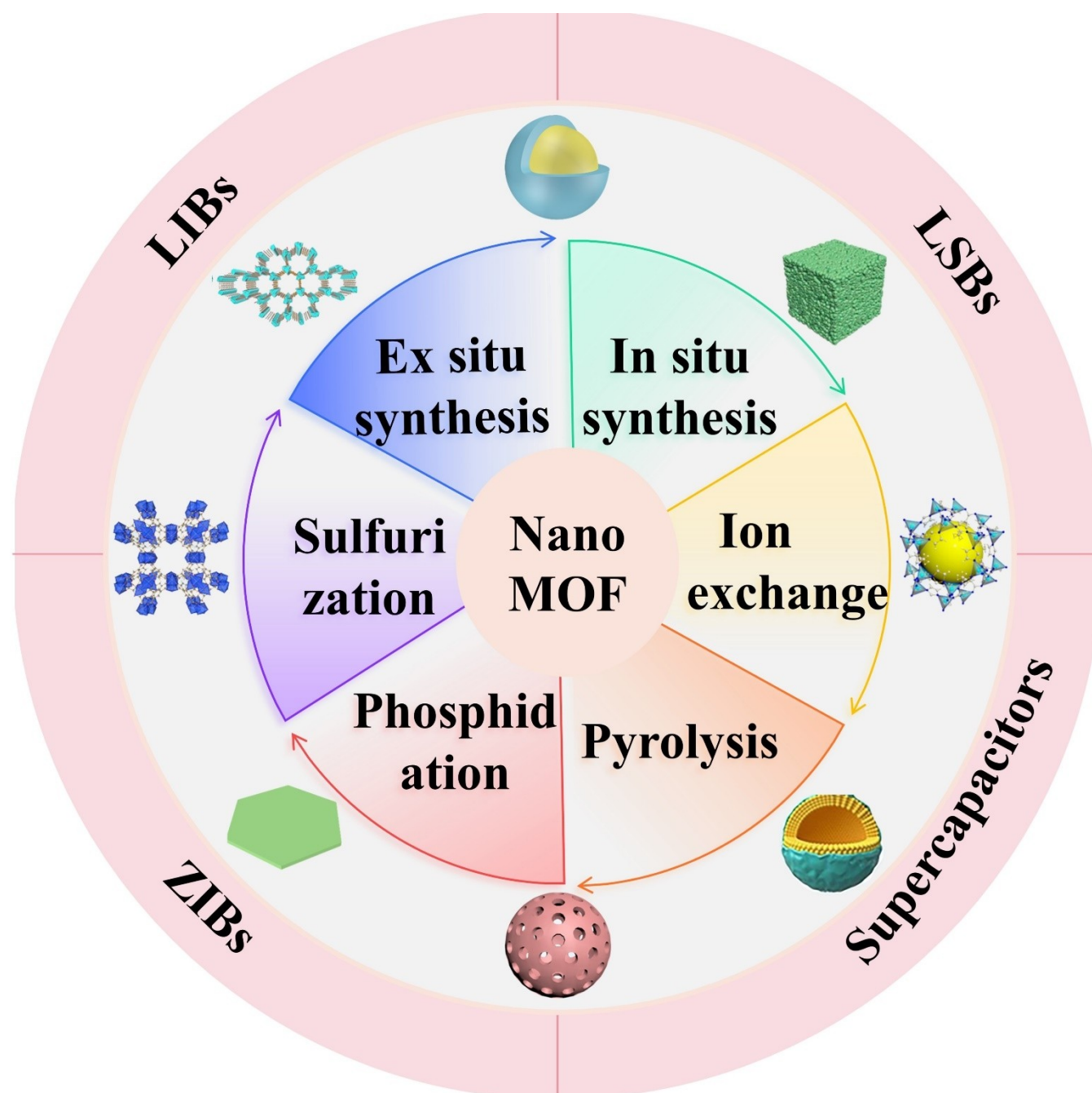# Nano Metal–Organic Frameworks as Advanced Electrode Materials in Electrochemical Energy Storage

Xiaohui Wu,[a] Ziheng Fan,[a] Jinliang Hu,[b] Yan Yan,[c] and Huan Pang*[a]

Batteries & Supercaps

Review
doi.org/10.1002/batt.202400064

Chemistry Europe
European Chemical
Societies Publishing

Nano metal–organic frameworks as an attractive new class of porous materials, are synthesized via metal ions and organic ligands. With their desirable properties of abundant pores, high specific surface areas, fully exposed active sites and controllable structures, nano MOFs are acknowledged to be one of the most vital materials in electrochemical energy storages. However, in their practical applications, nano MOFs are still confronted with various difficulties and challenges because of their low conductivity, poor stability, and other disadvantages. The selection and development of MOF composites, MOF–derived materials and modified MOFs might be beneficial to use as better electrode materials to greatly improve the electrochemical properties of energy storage devices. This paper mainly focuses on the recent developments of nano MOFs as prospective materials in electrochemical energy storage applications, including lithium–ion batteries (LIB), lithium–sulfur batteries (LSB), zinc–ion batteries (ZIB), and supercapacitors (SCs). Finally, the challenges faced by these kinds of energy storage devices are proposed, along with the current directions and prospect.

1. Introduction

Under the current situation of the great development of the world economic globalization,[1] owing to the pretty high speed of the development of industry and the rapid continuous increase in population, people rely on non–renewable energy to maintain the needs of production and life, resulting in an increasing energy demand.[2,3] Fossil resources have been exploited, burned, and discharged in large quantities, resulting in serious environmental pollution and energy shortage.[4] To protect the ecological environment and solve the problem of depletion of fossil fuel resources, the immediate priority is to look for sustainable energy technologies, including the development of clean energy (wind, solar, hydropower) and the use of renewable energy (nuclear energy, biomass energy).[5,6] The instability of these energy sources makes energy storage necessary.[7,8] Current electrochemical energy storage systems mainly include fuel cells, rechargeable batteries (lithium–ion batteries, lithium–oxygen batteries, and sulfur–ion batteries), and supercapacitors.[9] Among them, batteries and supercapacitors are the most efficient and applicable electrochemical energy storage devices. For instance, the REDOX reaction of LIBs electrode materials can be promoted to provide a high energy density by the insertion of lithium ions. There are two main types of supercapacitors according to the charge storage mechanism.[10] Electric double–layer capacitors (EDLCs) store electrical energy in the form of static electricity. When the electrode is charging, the static charge accumulates on the electrode surface, attracting the opposite ions in the surrounding electrolyte solution, so these ions attach to the electrode surface, forming a double layer capacitor.[11] Pseudo–capacitances are based on a reversible REDOX reaction between electrodes and electrolytes. The reason for the wide applications is because of its density, excellent performance, high chemical stability, and structural stability.[12] However, it still does not meet the growing needs of people.[13] Electrode materials largely determine the performances of batteries and supercapacitors. However, they generally have the shortcomings of low capacitance and poor stability. Thus, it is crucial to select and develop better energy storage devices with lower cost, longer cycle life and other attractive advantages via designing new electrode materials.[14]

As a sort of porous crystal materials, nano metal–organic framework materials are synthesized via metal clusters/ions and organic ligands through coordination bonds.[15,16] Nano MOFs show great potential in various fields such as sensing, water treatment and energy storage due to their advantages of large specific surface area, adjustable structure, and controllable composition.[17,18,19,20] At present, nano MOFs are principally divided into three categories: original MOFs, MOF composites and MOF–derived materials. Original MOFs are recognized as functional materials owing to their attractive properties of high porosity, excellent customizability, and controllable structures.[21] However, its inherent low conductivity and electrochemical stability are still the limitations and obstacles to achieve large–scale application.[22] Interestingly, a strategy has been found to make best use of the advantages and bypass the disadvantages of primitive MOFs, namely, to compound them with conductive substrates or functional materials (such as conductive polymers, and graphene).[23] They can also be modified by improving synthesis methods or packaging some materials. In addition, partial MOF–derived materials[24,25,26,27] also show excellent electrochemical properties, arousing people's interest.[28]

In this review, we mainly focus on the recent developments of nano MOFs in various batteries and supercapacitors (Scheme 1). Furthermore, some unconquered challenges are summarized, and basic solutions are put forward at the end.

[a] X. Wu, Z. Fan, Prof. H. Pang
School of Chemistry and Chemical Engineering, Yangzhou University
Yangzhou, 225009, Jiangsu, P. R. China
E-mail: huanpangchem@hotmail.com
        panghuan@yzu.edu.cn

[b] J. Hu
Jiangsu Yangnong Chemical Group Co. Ltd.
Yangzhou, 225009, P. R. China

[c] Y. Yan
Yangzhou University Library, Yangzhou University
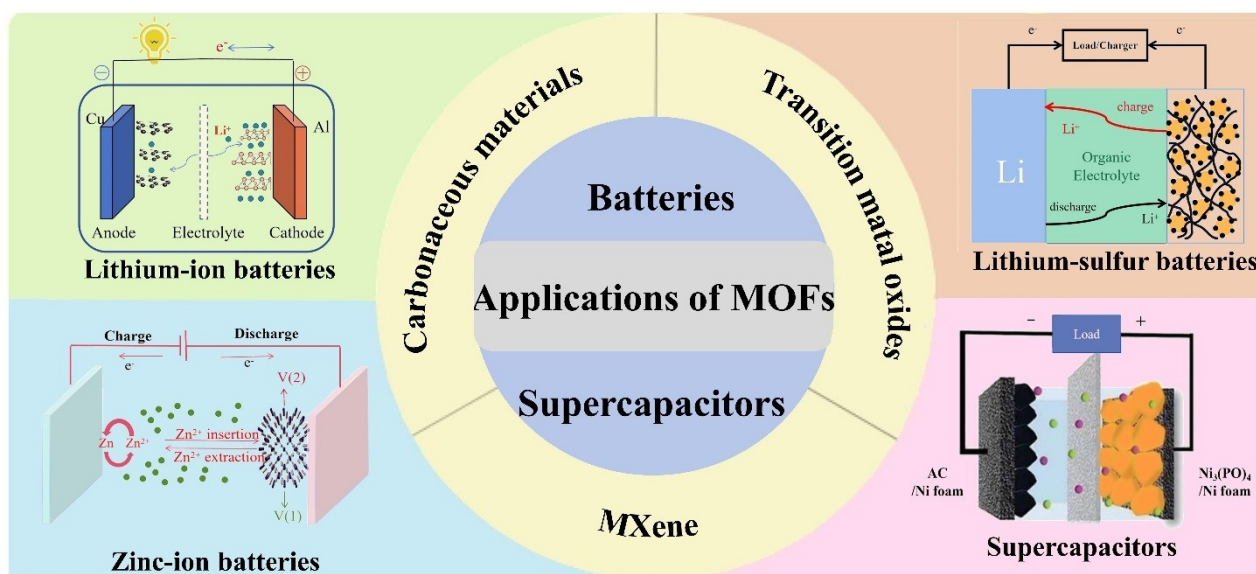Yangzhou, 225009, Jiangsu, P. R. China

2. Batteries

Batteries, because of their environmental friendliness, outstanding properties, and long cycle life, are one of the most widely used and vital energy storage devices. They can minimize the dependence on non–renewable energy and achieve the storage of renewable energy.[29] Nevertheless, they still face many difficulties and challenges. Their safety, energy density, cycle life, and other electrochemical performances have been unable

Scheme 1. Illustration of applications of nano MOFs in batteries and supercapacitors.

to meet people's needs. For instance, in the field of aerospace and new energy vehicles, better batteries are needed.[30] In recent decades, nano MOFs have been extensively studied to enhance batteries' properties.

2.1. Lithium–Ion Batteries

Lithium–ion batteries (LIBs) arouse people's attention on account of their good stability, high working voltage, and other excellent properties.[1,31] However, expansion and contraction during lithiation lead to the formation of cracks that destroy the electron–conducting network of the electrode.[32] At the same time, LIBs have limited theoretical capacity, which can no longer meet the needs of people's production and life. Electrode materials have been proven to be one of the most critical components of LIBs.[33] However, common anode materials have many disadvantages.[34] To further design active materials with excellent performances for LIBs, people turn attention to nano MOFs. Nano MOF–derived materials that can help overcome the expansion during lithiation are the key to improve the performances of the electrodes. Besides, cathode materials determine the cost and energy density of LIBs. There are three primary kinds of commercialized traditional cathode materials: lamellar cathode, spinel cathode and olivine cathode.[35] The application of MOFs in cathode materials often faces structural collapse, while PBAs, as a branch of the MOFs family, have many sites, and are the main force of new positive electrode materials. Scheme 2 displays the pros and cons of different electrode materials for LIBs.
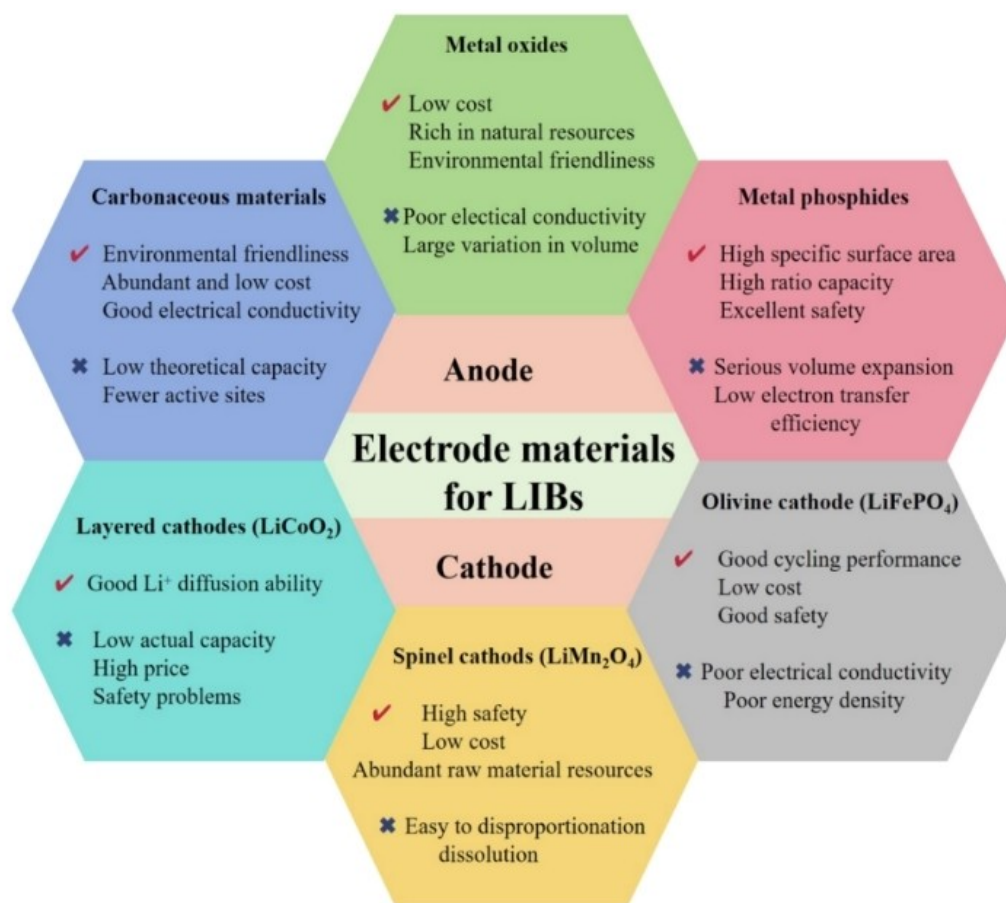
2.1.1. MOF/Carbonaceous Materials

Carbonaceous materials combined with nano MOFs both retain the advantages of MOFs and use the conductivity of carbonaceous materials to overcome the limitation of original MOFs. Due to their outstanding carrier mobility and desirable stability,

Xiaohui Wu is now a student under Professor Huan Pang's supervision, at School of Chemistry and Chemical Engineering, Yangzhou University, China. Her main research interests are in the field of energy storage materials, including supercapacitors and ion batteries.

Huan Pang received his Ph.D. degree from Nanjing University in 2011. He is now a distinguished professor at Yangzhou University, a Young Changjiang Scholar of the Ministry of Education in China, and a senior member of the Chinese Chemical Society. He is the managing editor of EnergyChem, the editorial board member of ElatChem and Rare Metals, and the youth editorial board member of Nano Research, Nano Research Energy, and eScience among other distinguished academic journals. He was recognized as a highly cited researcher in Cross-Field by Clarivate Analytics in 2020 to 2022. His research area mainly focuses on MOFs related materials.

Scheme 2. The pros and cons of different electrode materials for LIBs.

MOF/carbonaceous materials have been widely used in LIBs. Table 1 exhibited the reversible capacity, current density and initial coulombic of MOF/Carbonaceous materials and their derivatives. Graphene, as a two–dimensional (2D) carbon nano-sheet with a conjugated hexagonal lattice of sp^2 hybrid carbon, is a traditional electrode material for LIBs.[36] The combinations of graphene with MOFs have been recently confirmed that they can not only avoid the aggregation and reaccumulating phenomenon between graphene sheets, but also provide anchor points for MOFs through strong interactions. The disorder of MOF crystalline structure results in the formation of more channels during the cycle, and Li^+ is effectively diffused through the plug–in lithium storage mechanism.[37] Moreover, graphene oxide (GO) has rich surface oxygen–containing functional groups and attractive ionic conductivity. However, the traditional GO cannot be directly applied as electrode materials because of its hindrance effect on lithium ions and surface state. Nano MOF/GO derivatives prepared by the precursor system are widely used in LIB electrodes.[38] For example, Co–MOFs/GO composites are prepared by a simple solvother-mal reaction. Owing to the majorization of GO morphology and layer structure, Co–MOFs/GO composite electrode exhibits an outstanding specific capacity of 569.50 mAh g^{-1} at the current density of 500 mA g^{-1}. This material can maintain remarkable

specific capacity at 1000 mA g^{-1} after 500 cycles. Graphene nanosheets (GNS) are a new sort of nanomaterials with 2D layers of one–atom thickness that form a strongly bonded carbon network.[39] The reported 2D Ni_7S_6/GNS as anodes in LIBs delivered a high initial capacity of 630 mAh g^{-1} and maintain a remarkable reversible capacity of 510 mAh g^{-1} after 30 cycles.[40] Reduced graphene oxide (rGO) is another attractive carbona-ceous material for LIBs. Although it cannot achieve high electrical conductivity due to its incomplete structure compared with graphene, its combination with nano MOF has unexpect-edly demonstrated excellent electrochemical properties. Fe–MOF/rGO and the main synthesis progress were reported by Jin and colleagues.[41] First, rGO was added to DMF, followed by stirring to ensure complete dispersion. Then, $C_8H_6O_4$, $FeCl_3 \cdot 6H_2O$, and glacial acetic acid were added to the solution one by one. The final product was obtained by transferring the mixture into a Teflon–lined autoclave. When Fe–MOF, Fe–MOF/rGO (5%), and Fe–MOF/rGO (10%) were applied in LIBs, the electrochemical performance tests exhibited impressive results. With the addition of rGO, the irreversible reaction is gradually reduced, while the capacitance and cycle stability are improved. In recent years, Ni–rich layered cathode materials, especially $LiNi_{0.8}Co_{0.1}Mn_{0.1}O_2$, are taken for promising cathode materials. However, its poor rate capacity and cycle stability further hinder

Batteries & Supercaps

Review
doi.org/10.1002/batt.202400064

Chemistry Europe
European Chemical
Societies Publishing

Table 1. MOF/Carbonaceous materials and their derivatives for LIBs.

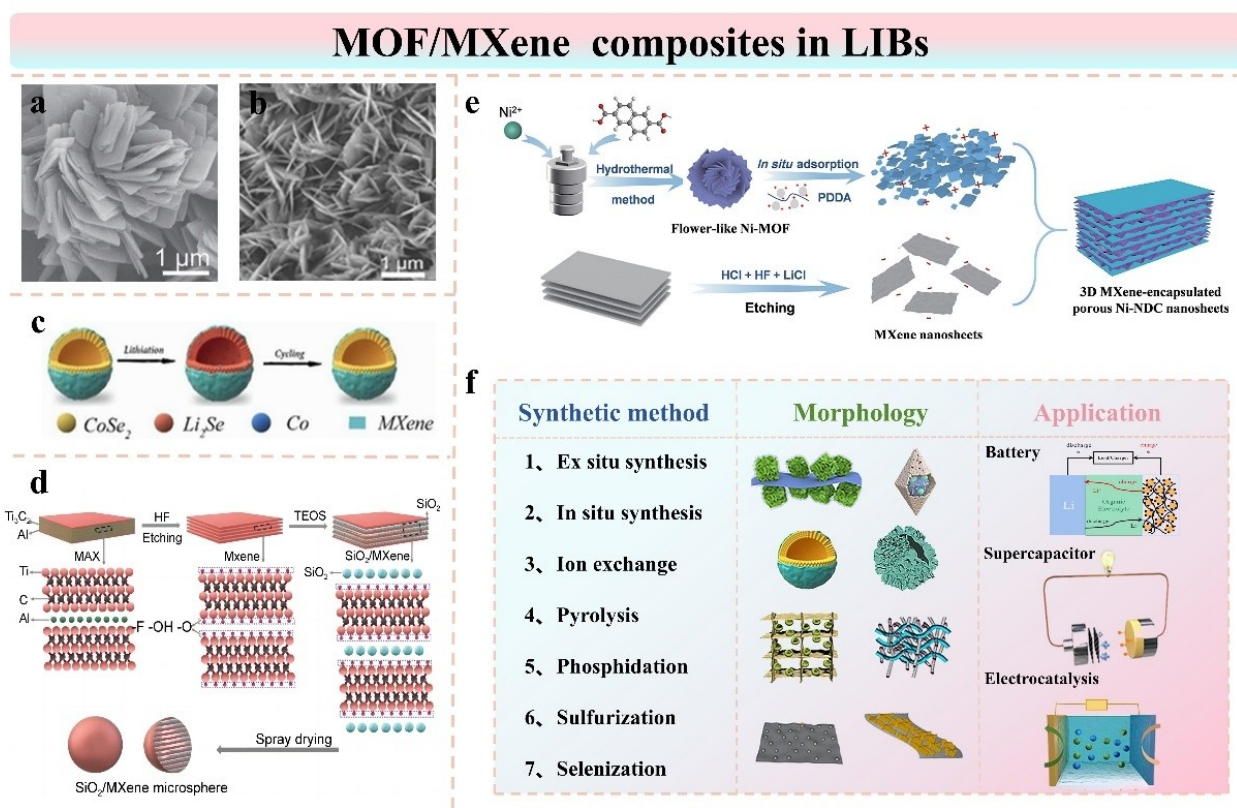| Materials	Reversible capacity (mAh g^{-1})	Current density (mA g^{-1})	Initial Coulombic Efficiency (100%)	Ref.
Ni/Ni$_3$S$_2$/GO	1011	100.0	90.6	[29]
NiMn$_2$O$_4$/rGO	1815	100.0	80.6	[29]
ZnO/ZnFe$_2$O$_4$/C	1385	0.500	–	[30]
ZnCoS@Co$_9$S$_8$/N–doped C	1813	500.0	–	[30]
Fe$_2$O$_3$/Co$_3$O$_4$/rGO	1110	1.000	–	[35]
Fe$_3$O$_4$/NC@rGO	1379	0.100	–	[35]
Fe$_3$O$_4$@C	1714	0.100	–	[35]
MoO$_2$/ZnSe@N–C	1126	0.100	–	[35]
SnO$_2$@MOF/graphene	450.0	1000	47.0	[37]
Co(L)MOF/rGO	206.0	500.0	98.0	[37]
Fe–MOF/rGO (5%)	1010	500.0	43.3	[37]
Al–MOF/graphene	400.0	100.0	–	[38]
NC/graphene	1301	100.0	–	[38]
Co–MOF/rGO	367.0	200.0	–	[38]
Fe$_2$O$_3$/rGO	846.9	500.0	–	[38]
NG@SnSe/C	650.0	50.00	–	[38]
3DG/FeS@C	632.0	100.0	–	[38]

commercial application. According to the existing research, the cycle stability can be enhanced by designing core–shell or hollow nano structures.[42] To improve its conductivity, Jan with his co–workers tried to modify LiNi$_{0.8}$Co$_{0.1}$Mn$_{0.1}$O$_2$ wrapped with graphene nanosheets to obtain LiNi$_{0.8}$Co$_{0.1}$Mn$_{0.1}$O$_2$-graphene composite material.[43] Electrode dynamics are significantly enhanced by introducing graphene nanosheets, facilitating the transfer of Li$^+$, as well as the transfer of electrons from the collector to the active material. The present composite electrode displays a better rate capability of 163 mAh g^{-1} and remarkable cycling stability. The capacity retention is still outstanding to be 92% over 150 cycles.

In summary, MOF/Carbonaceous materials are always obtained via the hydrothermal method, the solvothermal method, and others. Their frame structure can be maintained during Li insertion. At the same time, the volume strain is also very small, which allows the electrons and Li$^+$ transport molecules to self–assemble. These strengths further promote their developments in LIBs. Although much progress has been made for LIBs in recent years, there is still plenty of room to design more materials with better performances, which requires a better understanding of the lithium storage mechanism.

2.1.2. MOF/MXene Composites

Since graphene was discovered, two–dimensional layered materials have attracted more researchers because they have high electrical conductivity and remarkable cycle stability. Many new two–dimensional nanomaterials have been successfully prepared and widely used, such as black phosphorus, 2D transition metal carbides, 2D metal sulfides and nitrides, silene and metal oxides.[44] As new two–dimensional transition metal carbides and nitrides, MXenes have received people's attention due to their superior electrical conductivity, unique surface hydrophilicity, and excellent mechanical properties.[45] The general chemical formula for MXene is $M_{n+1}X_nT_x$ (n = 1–4), where M is on behalf of transition metal (such as Nb, V, Ti, etc.), X stand for C or N, and T is the surface end group (–O, –OH, and/or –F) produced during etching. Notably, MXenes, with its ultra–high–volume capacitance of up to 1500 F cm^{-3}, is considered an effective substrate for improving the stability and conductivity of nano MOFs. However, MXenes still suffer from oxidative degradation and self–re–cracking, leading to the collapse of the two–dimensional structure, which seriously deteriorates its performance and hinders further applications. To overcome these shortcomings, lots of studies have been carried out on synthesis strategies, morphology, and related developments of MOF/MXene composites and their derivatives as shown in Figure 1f. With the rapid development of nano-technology, people have a further understanding of nano MOFs.[46] Zhu and colleagues reported a method of polymerizing and hybridizing ultrathin Ti$_3$C$_2$MXene and three–dimensional (3D) Ni–NDC nanosheet aggregates to successfully synthesis MXene–encapsulated porous Ni–naphthalene dicarboxylic acid (Ni–NDC) nanosheets.[47] The synthetic procedure is mainly demonstrated in Figure 1e. A 3D flower–like Ni–NDC structure can be seen through the SEM images of Ni–NDC (Figure 1a). In accordance with the working mechanism of LIBs, Li$^+$ ions are primarily inserted and extracted into the organic components of MOFs. Owing to the interaction effects of Ni–NDC and MXene, the product could avoid self–agglomeration and buffer the volume expansion of Ni–NDC nanosheets. The obtained anode could achieve a high specific capacity of 579.8 mAh g^{-1} at 100 mA g^{-1} over 100 cycles. It also enhanced long–term cycle capability and magnification capability. In addition, conductive MOFs with outstanding structural stability and attractive REDOX properties were hybridized with MXene[48] to obtain a nickel–ferrocene dicarboxylic MOF (NF–MOF)/Ti$_3$C$_2$T$_x$MXene (NF–MOF@MXene) heterostructures (Figure 1b). It can be observed that NF–MOF nanosheets are uniformly grown on MXene nanosheets. When using the final product as the anode material, it retained a high capacity of 80% even over 5000 cycles. The fast Li$^+$ insertion/extraction kinetics of NF–MOF@MXene may be due to the enhanced Li$^+$ adsorption energy caused by the interaction. According to the report, the core–shell structures have appealing topologies and predominant chemical performances. They can be used as a template for later preparation of hollow architectures. Designing hollow structures or core–shell nanocomposites is another efficient method. Mixing spherical Co–MOFs with selenium powder, treating to prepare hollow CoSe$_2$ spheres, and then further hybridizing them with MXene via an electrostatic self–assembly way.[48] CoSe$_2$@MXene hybrids were obtained, which have the hollow–shell porous structure and the optimized electron/ion transport. The material exhibited an excellent rate performance

Batteries & Supercaps

Review
doi.org/10.1002/batt.202400064

Chemistry Europe
European Chemical
Societies Publishing

Figure 1. a) SEM images of Ni—NDC. b) SEM image of NF—MOF@MXene. c) Schematic diagram of the cycling stability of CoSe$_2$@MXene. d) Schematic illustration of the preparation of SiO$_2$/MXene microspheres. e) Schematic illustration of the preparation of 3D MXene–encapsulated porous Ni-NDC nanosheets. f) Schematic illustration of the main synthesis methods, morphology, and applications of MOF/MXene composites and their derivatives. Panels a and e: Reproduced with permission.[47] Copyright 2022, Springer. Panels b and c: Reproduced with permission.[48] Copyright 2023, American Association for the Advancement of Science. Panels d: Reproduced with permission.[49] Copyright 2021, Youke Publishing.

of 465 mAh g^{-1} and a cyclic property over 1,000 cycles at the current density of 5 A g^{-1} (Figure 1c). In addition, SiO$_2$ nano-particles are found to prevent the re–stacking of MXene flakes, make the entire microsphere structure more stable, and shorten the path length of Li$^+$. Through combining spray drying, the Bai group obtained SiO$_2$/MXene microspheres[49] as shown in Figure 1d. Firstly, prepare laminated MXenes (Ti$_3$C$_2$T$_x$) via using HF acid selectively etch the Al layer in the MAX phase. Then, grow SiO$_2$ nanoparticles on the MXene sheet. At final, the final product was synthesized via the spray–drying method. The outside is a flexible MXene film wraps, while the inside is a stacked MXene–SiO$_2$—MXene structure. Thus, the microsphere SiO$_2$/MXene hybrid material as the anode in LIBs displayed attractive electrochemical performance with an outstanding capacity of 838 mAh g^{-1} at the current density of 100 mA g^{-1}.
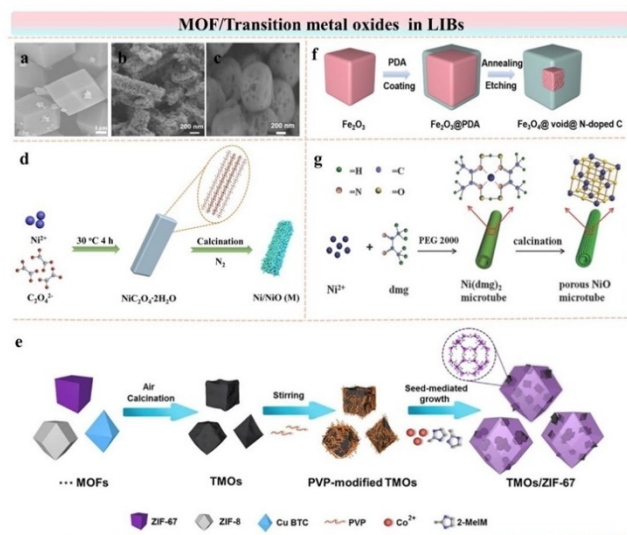
In sum up, designing MOF/MXene composites and their derivatives for high electrochemistry properties and superior lithium storage has achieved more attention. Various MOFs including Ni–MOF, PBAs, etc. have been compounded with MXenes via situ synthesis and exsitu synthesis. Many MOF–derived TMOs and TMPs have been combined with MXene to design better batteries. In general, introducing MXene nano-sheets uniformly into MOF not only efficiently avoids the aggregation of MXene nanosheets but also slow down the

volume expansion during the rapid Li$^+$ insertion/extraction process. Also, it can provide adequate active areas for facilitating further electrolyte penetration. Therefore, MXene/ MOFs and their derivatives offer broad prospects in improving electrochemical properties because of their useful synergistic effects.

2.1.3. MOF/Transition Metal Oxides (TMOs) and Derivatives

Typical transition metal oxides (TMOs) include RuO$_2$, Co$_3$O$_4$, NiO, Mn$_2$O$_3$, etc.[50] The conversion reaction between lithium ions and transition metal oxides is M$_x$O$_y$+2yLi$^+$+2ye$^-$=yLi$_2$O+xM. Their specific capacity is higher than graphite when applied in LIBs. (Table 2) The high cost of RuO$_2$ has limited commercial applications and encouraged the search for alternative useful materials at low cost. Another two transition metals, Nb and Ta have been limited because of low electronic conductivity, high cost, and rarity.[51] For Co–MOF, lots of studies have shown that MOF/Co$_3$O$_4$ composites are strong competitors for lithium–ion battery electrode materials. For example, Zhang et al. tried to compound Co$_3$O$_4$ with ZIF-67, using seed–mediated growth method to fix free Co (II) ions to PVP pre–modified TMOs seeds,

Batteries & Supercaps

Review
doi.org/10.1002/batt.202400064

Chemistry
Europe
European Chemical
Societies Publishing

and then added 2-methylimidazole ligands to form ZIF-67 crystals with exposed Co (II) ions[52] (Figure 2e). ZIF-67 is a kind of Co–based MOF that exhibits crystalline multi–porosity as MOF and chemical stability as zeolites. ZIF-67 coating prevents exposing Co_3O_4 directly to the electrolyte, additionally, relieves the volume of Co_3O_4 during cycling and benefits the rapid ion insertion–disinsertion. Therefore, Co_3O_4/ZIF-67 composites (Figure 2a) have bright prospect and significant potential in the electrochemical energy storage filed. To improve the volume change, ion diffusion and other problems of LIBs, designing unique structures such as hollow and porous is an effective method. Huang prepared Co_3O_4/NiO composites with MOF and added carbon to obtain yolk @ shell NiO–Co_3O_4@C (YNCC) composites.[53] Even more attractive and unique, due to their inherent material and structural characteristics, the final products show better cycle stability and excellent rate capability. Using Co—MOF as a precursor to synthesis porous materials is a wonderful thought. Li et al. came up with an idea as to synthesis mesoporous $Ni_xCo_{3-x}O_4$ nanorods. Via a one–step microwave–assisted synthesis, they successfully prepared by using Co/Ni MOF as a precursor.[54] The obtained electrode exhibits high cycle performance and significant capacity retention even at different high current rates. At the same time, transition metal oxalates are a kind of coordination compound with some characteristics of MOFs, which have brought about widespread attention because of their controllable structure and pore size.[55] Transition metal oxalates and their derived materials are commonly used to prepare precursors for LIBs. They can shorten ion diffusion channels, increase active sites,

Table 2. MOF/Transition metal oxides (TMOs) composites and their derivatives for LIBs.

Materials	Reversible capacity (mAh g^{-1})	Current density (mA g^{-1})	Initial Coulombic Efficiency (100%)	Ref.
Co_3O_4/ZIF-67	720.0	1000	–	[52]
Co—BDC MOF	1090	200.0	–	[54]
Co—BTC MOF	>750.0	100.0	–	[54]
FeO/NiCo$_2$O$_4$	734.0	1.000	85.8	[56]
Fe$_2$O$_3$ microboxes	1180	200.0	72.0	[59]
Hollow Fe$_2$O$_3$ spheres	1255	500.0	67.0	[59]
H—Co—MOF	1345	100.0	99.0	[60]
Co$_2$(OH)$_2$BDC	650.0	50.00	99.0	[60]
Ni—BTC	1085	100.0	96.4	[60]
NiCo$_2$O$_4$/C	889.0	200.0	–	[61]
NiCo$_2$O$_4$/NiO	1535	200.0	–	[61]
Fe$_3$O$_4$@N–doped C	1222	200.0	–	[62]

accelerate reaction kinetics, and thus achieve excellent electrochemical properties. Porous Co_3O_4 was successfully obtained via a simple pyrolysis of a cobalt oxalate precursor by Yuan and Che group, which has large surface area, high surface permeability and other advantages for rapid diffusion and volume change of Li$^+$. Transition metal cobalt salts have many merits providing them with higher specific capacity, such as a variety of oxidation states, active centers, and complex structures. When made into different nano materials, the higher specific surface area and conductivity make the electrochemical performance further improved. Furthermore, the abundant lithium energy storage sites on the surface can greatly reduce the volume expansion during the lithium insertion/extraction process and obtain excellent cycle and rate performance. Ni—MOF has been claimed as a competitive candidate in the energy storage because of its low cost, environmental benignity, and natural abundance. The Fu group obtained porous NiCo$_2$O$_4$ microrods and microspheres.[56] Nevertheless, pure Ni—MOFs have not been widely used because of their low electrical conductivity. Some methods are put forward and applied to overcome the limitation of pure Ni—MOFs: (1) By improving the synthesis conditions or looking for new synthesis strategies, find suitable ligands and adjust the structures.[57] (2) By using Ni—MOFs as precursors, prepare high–performance derivatives via high–temperature pyrolysis, calcination, or other methods. (3) By introducing other metal ions or functional materials. Among Ni–based materials, NiO is one of the most vital materials used in LIBs. However, manifests substantial volume changes, aggregation, and low conductivity usually trigger severe capacity attenuation and encumber its practical applications. Various NiO nanostructures, including nanowires, nanosheets, and nanofilms, have displayed great potential. On this basis, Li with co–workers synthesized porous Ni/NiO(M) nanocomposites by directly calcining nickel oxalate precursor at 30°C for 4 h and adjusted the Ni (0) content[58] as shown in Figure 2d. They found that a porous M-2 electrode with a Ni (0)
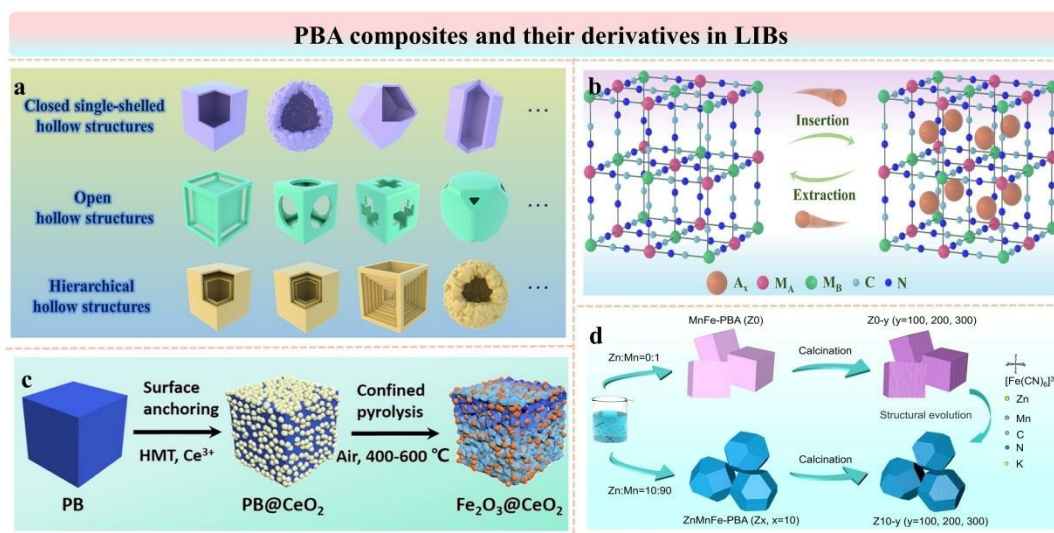

Figure 2. a) The SEM images of Cubes-300/ZIF-67-A composite. b) The SEM images of M-2. c) The SEM images of Fe$_3$O$_4$@N–doped C sample. d) Schematic diagram for the two–step fabrication route of the M samples. e) Schematic illustration for the fabrication of TMO/ZIF-67 composites. ("…" represents different MOFs) f) Schematic illustration of the synthesis process of Fe$_3$O$_4$@void@N–doped C. g) Schematic program for the formation of porous NiO microtubes. Panels a and e: Reproduced with permission.[52] Copyright 2022, Elsevier. Panels b and d: Reproduced with permission.[58] Copyright 2020, Elsevier. Panels c and f: Reproduced with permission.[62] Copyright 2022, MDPI. Panels g: Reproduced with permission.[59] Copyright 2018, Wiley.

mole ratio of 17.9% could obtain an outstanding capacity of 633.7 mAh g^{-1} at a current density of 0.2 A g^{-1} after 100 cycles. The design and fabrication of a Ni/NiO nanostructured (Figure 2b) anode show extreme promise toward realizing high charge/discharge rate and long cycle life. Moreover, Yang and colleagues succeeded preparing hierarchically porous NiO microtubes through a simple precipitation strategy as shown in Figure 2g.[59] The final product exhibited a remarkable initial discharge capacity of 1180 mAh g^{-1} at 200 mA g^{-1}. Moreover, at a current density of 1000 mA g^{-1}, it still delivered a high reversible capacity of 640 mAh g^{-1} over 200 cycles. In addition, with many advantages of low cost, high theoretical capacity, abundant resources, and pollution–free properties, iron oxide is a kind of potential and prospect electrode materials for LIBs. However, during the lithium insertion process, the iron oxide exhibits a large volume expansion, which leads to poor cycling performance. Compared with ordinary materials, the layered nanostructured materials are superior because they have higher specific surface areas and more active sites for REDOX reactions. Hu and co–workers designed an iron oxide/carbon nano-composite with a hollow core–shell structure[62] as shown in Figure 2c. Firstly, nano Fe$_2$O$_3$@polydopamine were prepared by using ferric trioxide nano cubes and hydrochloride as precursors. Secondly, the Fe$_3$O$_4$@N doped C composite was obtained through further carbonization treatment. Finally, the core–shell Fe$_3$O$_4$@Fe$_3$O$_4$@N doped C-x composites with different void sizes were prepared via the etching method of ferumoxide (Figure 2f). There is an appropriate clearance size between the carbon shell and the core of the tetroxide. This facilitates the diffusion of the electrolyte and the transport of lithium ions. It can also further slowdown the volume expansion of ferric oxide. The final materials obtained by etching with 2 mol/L hydrochloric acid solution for 5 h have good electrochemical

properties. The discharge capacity of Fe$_3$O$_4$@Fe$_3$O$_4$–doped C-x can highly reach 1222 mAh g^{-1} at 200 mA g^{-1}.

In conclusion, the more widely used MOF/TMOs in LIBs are Co—MOF and Ni—MOF composites and their derivatives. Preparative electrodes with unique structures such as porous or hollow core–shell structures were found to have greater potential to improve current state–of–the–art rechargeable batteries. Specific structures with more active sites can shorten the transport distance of Li$^+$ and improve electrochemical performance. To promote electrolyte penetration and the transport of Li$^+$, effectively reduce the volume expansion during Li$^+$ dissociation, increase the electron transfer rate, and provide unlimited possibilities for finding candidate electrode materials.

2.1.4. PBA Composites and Their Derivatives

Prussian blue analogues (PBAs) are a class of polynuclear metal cyanides with zeolite properties and a 3D open frame structure, with the formula A$_x$M$_y$ [M′(CN)$_6$]$_z$, where A stands for alkali metal cations such as Na$^+$, K$^+$, and M and M′ for bivalent or trivalent transition metal cations. Alkali metal ions and different valence transition metal ions can be replaced quickly in aqueous solutions and greatly facilitate lithium–ion insertion/extraction. The main process of ion insertion/extraction in PBAs is shown in Figure 3b. PBAs are promising LIBs electrode materials.[63] However, there are many lattice defects in their structures, resulting in poor cyclic stability and capacity utilization. Researchers typically combine them with TMOs as anode materials. Nevertheless, the large volume changes, the limited electron and ion diffusion dynamics, still limit their commercial developments. Therefore, improving anode materials for practical applications is an urgent problem. Due to the presence of

Figure 3. a) Schematic illustration of various hollow structures of Prussian blue and its analogs (PB/PBAs). b) Schematic illustration of ion insertion and extraction process in Prussian blue analogs (PBAs). c) Schematic illustration of fabrication of Fe$_2$O$_3$@CeO$_2$. d) Formation process diagram of the cubic samples Z0 and Z0-y (y = 100, 200, and 300) and truncated octahedral samples Z10 and Z10-y (y = 100, 200, and 300). Panels a and b: Reproduced with permission.[63] Copyright 2023, Wiley. Panels c: Reproduced with permission.[64] Copyright 2022, Elsevier. Panels d: Reproduced with permission.[66] Copyright 2022, Elsevier.

Batteries & Supercaps

Review
doi.org/10.1002/batt.202400064

Chemistry Europe
European Chemical
Societies Publishing

metal and organic parts, PBAs can be transformed into nano-structured materials by calcination in the working environment (N_2, O_2, etc.) to achieve more complex structures. This has prompted people to study Mn–PBA, Ni–PBA, Co–PBA and Fe–PBA to obtain PBA crystals with more ideal structures. Wang and co–workers proposed[64] that cerium oxide nanocrystalline CeO_2 was uniformly deposited on the surface of PBA via a surface anchoring strategy. At last, $Fe_2O_3@CeO_2$ was formed to expand the storage capacity of lithium (Figure 3c). The $Fe_2O_3@CeO_2$ obtained by annealing at 400 °C exhibits remarkable rate properties at different current densities. Li and colleagues applied the porous $FeMnO_3/Mn_2O_3$ hybrid to the anode material of LIBs, which displayed an outstanding capacity of 995 mAh g^{-1} at 200 mA g^{-1} after 170 cycles. When PBA is used as a sacrifice template, a variety of derivatives are available. The current PBA derivatives have open hollow, hierarchical hollow, core@shell, and other structures. (Figure 3a) PBAs have been widely used as precursors to prepare complex nano composites. These materials have a better lithium storage capacity than any single one. Compared with single–component materials, using PBA core–shell particle heterostructure for LIBs can obtain longer cycle life and higher capacity. Asakura et al. synthesized CuFe–PBA@NiFe–PBA, demonstrating the synergistic effect of heterogeneous structures on electrode capabilities, and proving that the core–@shell framework can increase the cycle life by stabilizing the surface of the cyanide structure and controlling the solid–phase changes induced by the core charge states.[65] The results show that the use of core–shell heterostructures is a viable way to improve the properties of coordination polymer ion storage materials. In addition, the Guo group tried to doping Zn in Mn–PBA and retained the pores for mass transfer by low–temperature calcination activation, and finally obtained a unique truncated octahedron ZnMnFe–PBA[66] (Figure 3d). Surprisingly, the material as an anode for LIBs provided a remarkable specific capacity of 519.3 mAh g^{-1} at 0.1 A g^{-1}. The capacity retention was still outstanding to be 99.9% even after 100 cycles. It solves the typical problems of low cycle stability and low–capacity utilization of PBAs and creates a new idea for designing new PBAs.
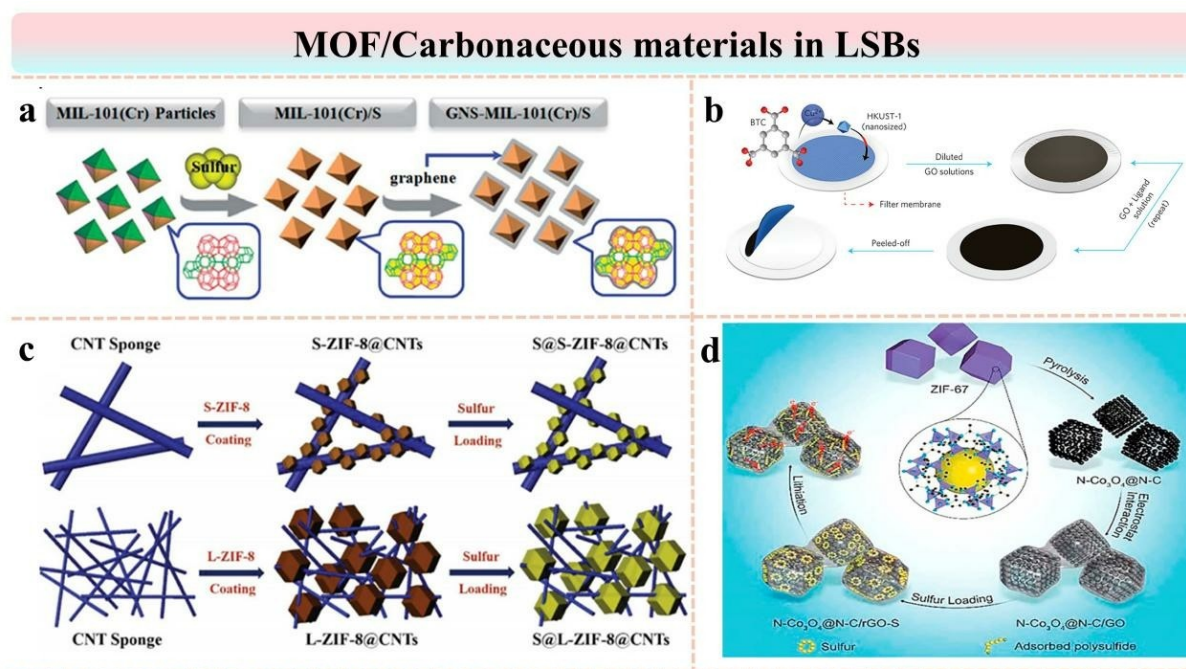
In a word, PBAs have been widely used in electrochemical energy storage in recent years, but their performance still needs to be further improved. The designs and applications of composite materials can greatly improve their electrical conductivity and stability. Composite materials can both reflect the advantages of all components and overcome the shortcomings still in existence. PBAs are usually combined with conductive polymers, and the electrochemical performance of the composites are significantly better than that of single PB and PBA. Improving synthesis methods (such as controlling the crystallization rate of PB, adding GO or in an inert gas environment to obtain more active sites) or creating core–shell heterostructures to improve the performance of coordination polymer ion storage materials provide feasible strategies for designing new PBA electrode materials.

2.2. Lithium–Sulfur Batteries

Lithium–sulfur battery (LSB) is a lithium battery composed of lithium metal as a negative electrode and sulfur as a positive electrode. Compared with LIBs, on the sulfur positive electrode in LSBs, each sulfur atom can accept two electrons to form S^{2-}, to achieve an outstanding theoretical energy density (2600 Wh kg^{-1}) and a remarkable theoretical capacity (1675 mAh g^{-1}). In addition, LSBs also have the advantages of environmental benefits and rich sulfur reserves. LSBs are therefore considered to be the promising and prospective energy storage devices. Nevertheless, owing to the insulation of sulfur and lithium sulfide, the "shuttle effect" caused by the diffusion of poly–lithium sulfide (LiPS), and the large volume expansion deformation during the battery cycle, the commercialization of LSBs has been hindered. At present, more and more studies are focus on MOF–based materials to overcome these limitations, especially by combining nano MOF with graphene and carbon nanotubes.

2.2.1. MOF/Carbonaceous Materials

Recently, carbonaceous materials have been widely used as common and powerful materials in LSBs. The combinations of nano MOF and carbonaceous materials are found to be efficient and prospective as the sulfur host. Graphene can accommodate a variety of nanoparticles and achieve high electrolyte contact area, and excellent electron transfer rate.[67] To further improve its performance, many studies have proposed to construct MOF/graphene composites with micro/nano porous structures. By a two–step method, Zhao group prepared the (GNS)-MIL-101(Cr)/S composite[39] (Figure 4a) as a suitable host for sulfur impregnation, which exhibits excellent capturing ability of the polysulfides. It has mesoporous cages, microporous windows, and a good conducting network. Moreover, MOF/graphene–derived metal phosphides are potential materials with broad application prospects due to their attractive theoretical capacity and activity. For instance, three–dimensional porous graphene was grown vertically on a flexible carbon cloth manufactured in situ to provide a good conductive network. CoP nanostructures were obtained by ZIF–derived to suppress the shuttle effect[38] to prepare CoP@G/carbon cloth and further promote the REDOX kinetics. The composite displays a remarkable capacity of 1044.9 mAh g^{-1} at 2.0 C, and the capacity decays only about 0.03% even after 500 cycles. Various modified graphene such as GO, rGO, and electrochemically reduced graphene oxide (ERGO) have been widely applied in LSBs. Bai group reported a new type of MOF battery separator synthesized by HKUST-1 and GO[37] as shown in Figure 4b. The interaction of MOF particles and GO laminates further enhanced the cycling stability of the separator. Therefore, the final product displayed a high retention rate of 99.7% even after 1500 cycles. ZIF-67 is a typical 3D topological MOF composed of Co^{2+} as the central ion and imidazolyl ligand. It has crystalline porosity, REDOX active center, high stability, and is the preferred template for preparing layered double hydroxides

Batteries & Supercaps

Review
doi.org/10.1002/batt.202400064

Chemistry Europe
European Chemical
Societies Publishing

Figure 4. a) Schematic diagram for the preparation of GNS–MIL-101(Cr)/S composite. b) Schematic illustration of the main preparation procedure of MOF@GO separators. c) The formation procedure of two typical hybrid structures. d) Schematic diagram for the synthesis process of N–Co_3O_4@N–C/RGO–S. Panels a: Reproduced with permission.[39] Copyright 2022, Elsevier. Panels b: Reproduced with permission.[37] Copyright 2022, Elsevier. Panels c: Reproduced with permission.[69] Copyright 2020, Elsevier. Panels d: Reproduced with permission.[38] Copyright 2022, Elsevier.

(LDH) with adjustable morphology and size. Due to the strong bonding between Li_2S_x and Co^{2+}, the Li_2S_x intermediate can be effectively captured, the "shuttle effect" can be suppressed, and its cycling performance and coulomb efficiency can be improved, but there are still problems of low conductance and volume expansion. Li and co–workers synthesized porous carbon polyhedral containing cobalt doping by carbonizing ZIF-67. By coating rGO on the surface of porous carbon polyhedron, the product rGO/C–Co–S can obtain special structure rich in mesoporous and microporous to fix sulfur. The rGO/C–Co–S cathode exhibits an outstanding specific capacity of 949 mAh g^{-1}. Meanwhile, the Xu group reported N–Co_3O_4@N–C/rGO, which was prepared by rGO coating N–Co_3O_4@N–C. Figure 4d demonstrates the main synthesis process. The capacity of this porous composite for LSBs cathode can highly reach 611 mAh g^{-1} at 2.0 C even after 1000 cycles. TMO@C materials with porous and hollow structures are also strong competitors of LSBs cathode materials. For example, the highly conductive porous octahedron Fe_3O_4@C was prepared from an in–situ carbon coating derived from MIL-53.[68] Its special porous structure facilitates electron transport and further improves the reaction kinetics. V_2O_3@C can also be derived from V–MOF (MIL-47). In addition, carbon nanotubes (CNTs) are superior to other nano carbon materials because of their unique 1D nanostructure, stable chemical properties, and excellent flexibility. Cao and co–workers grafted smaller and larger sized ZIF-8 nanoparticles onto CNT networks and obtained two distinct hybrid structures, S–ZIF–8@CNT and L–ZIF–8@CNT.[69] The synthesis procedures of two composites

are shown in Figure 4c. As using the two structures to manufacture electrodes after sulfur infiltration, S@L–ZIF–8@CNT was found to achieve better performance at about 800 mAh g^{-1} over 500 cycles. CNTs@ZIF–8 has recently been demonstrated to be controllably densified during room temperature drying. By systematically adjusting the ZIF-8 content, the dense monolithic CNTs@ZIF-8 utilized as a sulfur host exhibited volumetric capacity of 676 mAh g^{-1} when the ZIF-8 content achieved 70 wt%. The impact of pore size on the performance has been investigated by Mao et al.[70] HKUST-1, MOF-5, and ZIF-8, three different MOFs with different sizes are obtained and further researched. Among them, the S@HKUST-1/CNT cathode with a higher capacity of 1263 mAh g^{-1} at 0.2 C can retain 720 mAh g^{-1} even over 500 cycles.

In summary, due to their stable frame structure and rich active sites, MOFs can alleviate volume expansion and inhibit the "shuttle effect" in LSBs. Meanwhile, the micro/nanoparticle porous structure constructed by carbonaceous materials and MOFs can largely solve the problem of LSBs. Strategies such as using synergies between materials, finding easier synthesis methods, and replacing carbonaceous materials with better properties play a great role in the search for new MOF/carbon–based electrode materials.

2.2.2. PBA Composites and Their Derivatives

Prussian blue analogues have good properties such as unique nanopore and crosslinking channels, peroxidase–like activity,

Batteries & Supercaps

Review
doi.org/10.1002/batt.202400064

Chemistry
Europe
European Chemical
Societies Publishing

and controllable structure. The open metal centers in PBAs act as Lewis's acid sites with good affinity for negatively charged polysulfide anions, while the open frame structure allows efficient storage of sulfur and confinement of polysulfide lithium (LiPS). Although the original PBA has low initial capacity and poor cycling stability, it can be combined with functional materials to inhibit vacancy formation and improve electrochemical performance.

Wang and colleagues[71] prepared FeCoNi PBA nanotubes using a simple Ni/Co molar ratio of 1:3 co–precipitation process, then melted at 130 °C to introduce sulfur and diffuse it into the pores of the PBA. Finally, FeCoNi PBA–S–PPY composite was obtained by encapsulating polypyrrole (PPy) in FeCoNi PBA–S sample (Figure 5a). The synergistic adsorption effect on LiPS of the FeCoNi PBA made contribution to the strong adsorption ability, and the formation of physical barrier and the polar–polar bonds after combining with PPy can reduce the polysulfide diffusion, allowing full utilization of sulfur. (Figure 5b and c) Therefore, FeCoNi PBA–S–PPY can enhance the chemisorption of LiPS, minimize the shuttle effect, and achieve higher electrochemical performance. Su with co–workers prepared a Fe_3C@N–GE–carbon nanotube hybrid from low–cost PB.[65] One–dimensional (1D) carbon and two–dimensional (2D) graphene nanotubes are seamlessly integrated during the growth phase to obtain 3D nanostructures, which were subsequently converted to S@Fe_xS@N–GE–CNTs. The main formation procedure is displayed in Figure 5e. When used as a sulfur scaffold for LSBs, S@Fe_xS@N–GE–CNTs has an excellent reversible capacity of 1221 mA g^{-1} at 0.2 C, and the capacity of this material remained at 1014 mA g^{-1} over 100 cycles. The improved performance can be attributed to three–dimensional N–GE–carbon nanotube hybrid nanostructures. More defects were introduced in the experiment and the active site was effectively captured in the electroactive site within the cathode. This strategy opens new avenues for high–performance batteries. In addition, some studies on high–entropy oxides and MXenes found that introducing high entropy materials can reach high cycle performance, while high entropy in PBAs has not yet attracted attention. Inspired by this, Geng group[72] synthesized a PBAs library from binary entropy to high entropy based on five metal cations (Mn^{2+}, Co^{2+}, Ni^{2+}, Cu^{2+} and Zn^{2+}) and $K_3[Fe (CN)_6]$ by co–precipitation method with water as solvent (Figure 5d). High–entropy PBAs can act as a polysulfide immobilizer to inhibit the shuttle effect, and as a catalyst to promote the transformation of polysulfide. To further expand PBA materials, the controlled synthesis of PBA derivatives has also been explored. A series of metal oxides were prepared respectively, which retained their original cubic morphology. These samples are stable during the sulfur melt and impregnation process. The study confirmed the large interaction between sulfur and HE–PBA, as well as the suitability of HE–PBA as a sulfur carrier, which can be fixed in the cathode and inhibit the shuttle effect.

To sum up, there are few studies on PBAs as the sulfur main body in LSBs. When PBAs are applied in LSBs, there are the following advantages: First, as the Lewis acid site, the metal center has a good affinity with the negatively charged polysulfide anion, thus preventing the shuttle of polysulfide; Second, the open frame structure can fix the multi–lithium sulfide through the pore restriction effect, and alleviate the volume change during the battery cycle; Third, due to the stability of the structure, the geometry of PBAs hardly changes during ion insertion, which further alleviates the problem of capacity attenuation; Fourth, these compounds are constructed via a simple and inexpensive co–precipitation method using water as a solvent; Finally, PBAs are highly adjustable and can form a high–entropy material, providing more possibilities for achieving outstanding Li–S battery cathode materials. It is believed that PBAs will have greater development in lithium–sulfur batteries in the future.

Figure 5. a) Schematic illustration of the fabrication of the FeCoNi PBA–S–PPy. Schematic illustration of the adsorption of FeCoNi PBA-PPy on polysulfides: (b) pure sulfur cathode, (c) FeCoNi PBA–S–PPy cathode. d) Schematic illustration of the main formation process for PBA family from binary to high-entropy system by coprecipitation method at room temperature. e) Schematic illustration for preparing Fe_3C–N–GE–CNTs hybrids. Panels a, b and c: Reproduced with permission.[71] Copyright 2021, Elsevier. Panels d: Reproduced with permission.[72] Copyright 2022, Wiley. Panels e: Reproduced with permission.[65] Copyright 2017, Elsevier.

2.2.3. MIL Series

In recent years, MIL series, as a subclass of MOFs, are low cost, easy preparation, and non–toxic. Their intermetallic layer has a strong crystal texture, which can form various superstructures and arouse great interest in the scientific community. It is well known that the composition and structure, including the size and orientation of the crystal, affect the performance. Wang and colleagues prepared Fe_3O_4–doped porous carbon nanorods/3D kenaf stem–derived microporous carbon (ferric oxide–DCN/3D-KSPC) by pyrolysis annealing method. Experimental tests show that the product provides a high specific capacity of
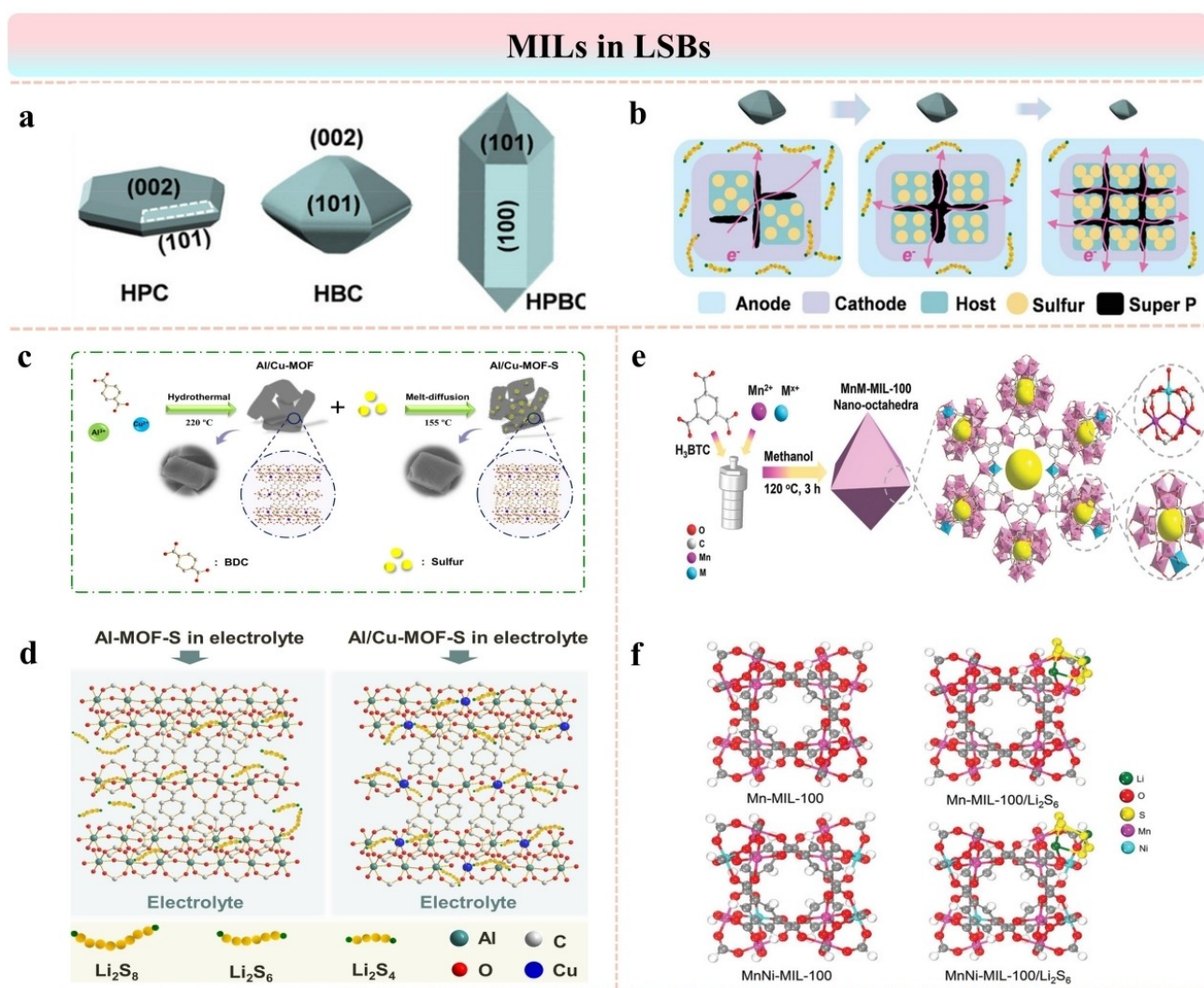
Batteries & Supercaps

Review
doi.org/10.1002/batt.202400064

Chemistry Europe
European Chemical
Societies Publishing

285.4 $F g^{-1}$ at 1 $A g^{-1}$. MIL-96-Al is composed of three–dimensional structure of Al octahedral unit and infiltration of 1,3,5-carboxylic acid ligands. Wang prepared different shapes of MIL-96-Al by co–solvent method,[73] including hexagonal platelet crystal (HPC), hexagonal bipyramidal crystal (HBC) and hexagonal prismatic bipyramidal crystal (HPBC) (Figure 6a). It is worth noting that as the crystal size decreases, the internal sulfur loaded in MIL-96 react more sufficiently. When the MOF crystal size decrease from microscale to nanoscale, the utilization of sulfur is improved. Particularly, during the GCD process, the HBC-0.78-S has the smallest charge–transfer resistance, and the resistance increases with increasing particle size. It is contributed to the inherent electrical conductivity determined by the contact area between the electrode materials and the conductive agent, as illustrated in Figure 6b. The Du group reported the publication of an Al–MOF–based bimetallic MOF,

commonly known as (Al)MIL-53.[74] (Al)MIL-53, forms a highly porous network and has a high pyrolysis temperature of 275 °C. However, Al^{3+} in Al–MOF is hexa–coordinated saturated and cannot bind to polysulfide. Developing bimetallic or polymetallic MOFs may be an effective strategy to inhibit the shuttle effect. They obtained Al/Cu–MOF as an advanced cathode material by uniformly dispersing Cu^{2+} in Al–MOF via a one–step hydrothermal strategy. The method on how to obtain Al/Cu–MOF–S is shown here in Figure 6c. When Al–MOF is used as the sulfur host, the generated Li_2S_x is almost completely dispersed in the electrolyte owing to the low–binding energy among Al^{3+}/Li_2S_x and few binding sites for Li_2S_x. In contrast, with Al/Cu–MOF as the cathode host materials, Li_2S_x molecules could be readily captured by Cu^{2+}, resulting from its strong binding energy and the lower steric hindrance (Figure 6d). As a result, the Al/Cu–MOF–n–S cathode exhibits higher specific
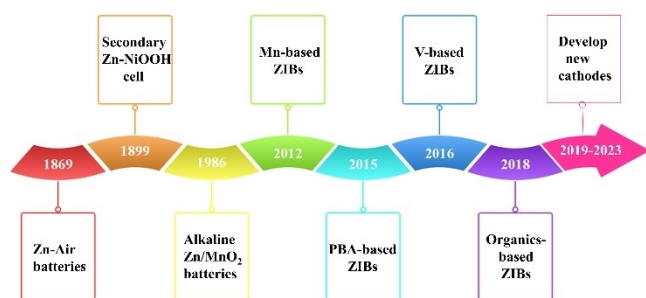

Figure 6. a) 3D representations of the crystal shapes and the (hkl) planes. b) Schematic illustration of the sulfur–loaded amounts, the contact area with conductive agent and the LPS distribution during the GCD process. c) Schematic diagram for synthesizing Al/Cu–MOF–S. d) Schematic diagram for the lithium polysulfides binding with Al–MOF and Al/Cu–MOF. e) Schematic diagram for the preparation of MnM–MIL-100 nano–octahedra. M represents the secondary metal ions incorporated into the metal–organic linker molecule. f) The structures of Mn–MIL-100, MnNi–MIL-100, and their complex with Li_2S_6. Panels a and b: Reproduced with permission.[73] Copyright 2022, Wiley. Panels c and d: Reproduced with permission.[74] Copyright 2021, Wiley. Panels e and f: Reproduced with permission.[75] Copyright 2021, Wiley.

Batteries & Supercaps

Review
doi.org/10.1002/batt.202400064

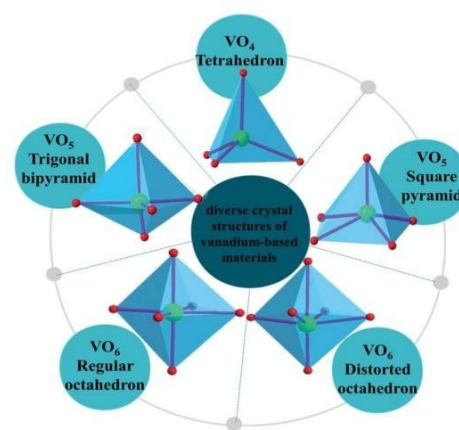**Chemistry Europe**
European Chemical
Societies Publishing

capacity and cycle performance than Al–MOF–S. Thus, the introduction of polymetallic gains is somewhat greater. For example, Guo et al. prepared a series of polymetallic Mn–based MOF nano octahedral MIL-100 crystals consisting of a super tetrahedral group based on trimeric acid and manganese trimer units.[75] They prepared monometallic Mn–MIL-100, bimetallic MnM–MIL–100 and trimetallic MIL-100 (MnNiCu–MIL–100 and MnNiCo–MIL-100) by solvothermal method (Figure 6e). The type and proportion of metal ions were adjusted reasonably without affecting the topological structure, and the cathode was prepared by using polymetallic manganese MIL-100 nano-meter octahedron as the main body of sulfur. First, compared with single MIL-100, active sites of bimetallic MIL-100 are much richer, and the electronic conductivity is higher. Second, the strong Lewis acid–base interactions between the Ni center and polysulfide anions are conducive to excellent battery perform-ance. (Figure 6f) Thus, LSBs assembled with MnNi–MIL–100@S cathode displays the better performance with a high specific capacity of 1579.8 mAh g^{-1}.

2.3. Zinc Batteries

In recent years, the increasing high cost, decreasing lithium resources, and serious environmental pollution have largely hindered the development of LIBs. While the energy storage/release mechanism of water zinc–ion batteries (ZIBs) is like that of traditional lithium batteries, and the insertion/extraction behavior of Zn^{2+} and the electron transfer efficiency determine the electrochemical properties of ZIBs.[76] Much research has been carried out on ZIBs, and the brief history is shown here (Scheme 3). Due to its abundant resources, high safety, and high theoretical capacity, ZIBs have been proven to be potential and prospective for the new generation of wearable electronic devices. Although ZIBs have many advanced features, the biggest obstacles are the relatively low capacity of the electrode materials[77] and the corrosion dendrite growth.[78] A great deal of works has been devoted to optimizing the performance of ZIBs, focusing on high–efficiency cathode materials, including such as manganese oxide–based materials,[79] Prussian blue analogs, and transition metal sulfides. Among these cathode materials, vanadium–based materials have received much attention because of their polyvalent adjustment ability (V (III), V (IV), V (V)).[80] In addition, as shown in Scheme 4, they have
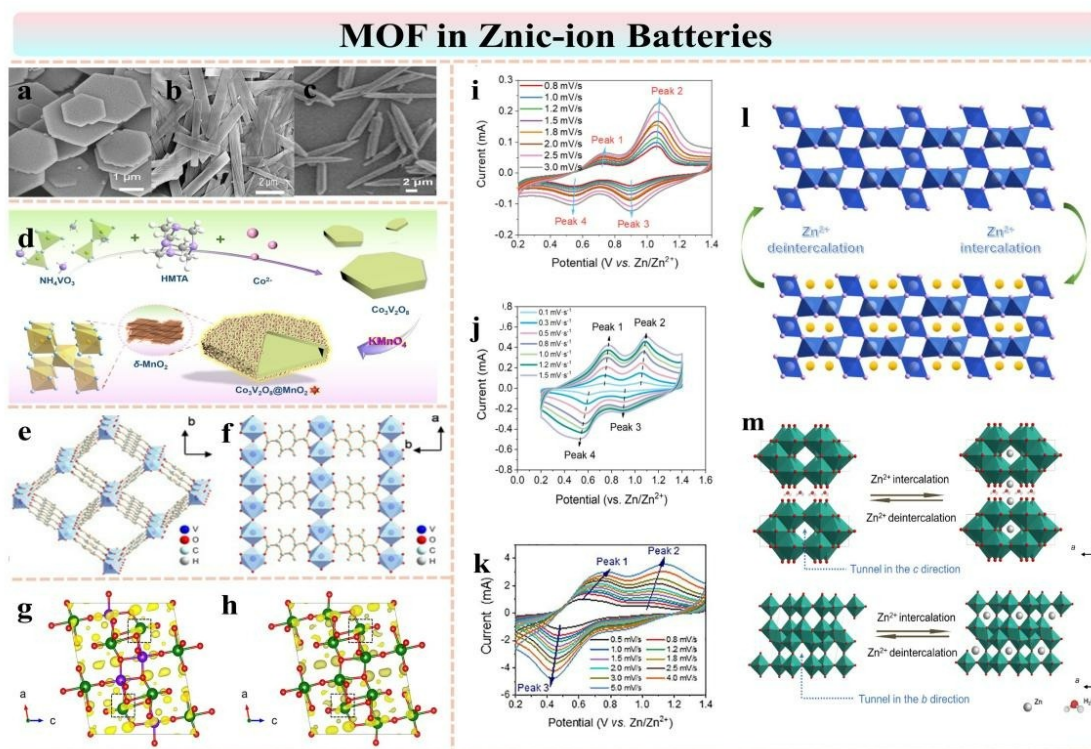
Scheme 4. Different vanadium coordination polyhedrons (Red O atoms, green V atoms, and pink V–O bonds).

diverse crystal structures, which can achieve electron transfer and alleviate the polarization problem.[81] As one of the representative members of the vanadium oxide family, VO$_2$, especially metastable VO$_2$(B), can promote the rapid diffusion of Zn^{2+} due to its unique tunnel structure, which can support better stability. Lv and his co–workers reported the preparation of nsutite–type VO$_2$ microcrystals as cathode materials through a mild hydrothermal reaction, using NH$_4$VO$_3$ as a precursor and thioacetamide as a reducing agent.[82] The CV curves (Figure 7i) at various scan rates were performed to further investigate the morphological details and electrochemical kinetics of the Zn//nsutite–type VO$_2$ microcrystals. The main synthesis procedure was shown (Figure 7l), and the mechanism demonstrates that the nsutite–type VO$_2$microcrystals allow the reversible intercalation/deintercalation of Zn ions. The VO$_2$ electrodes exhibited an attractive specific capacity (314.4 mAh g^{-1} at 1 A g^{-1}) with excellent power density (295.3 Wh kg^{-1} at 148 W kg^{-1}), as well as good stability with a capacity retention of 84 % even over 5000 cycles at 5 A g^{-1}. Many different methods have been applied to further improve the performance, such as reduction of the size and combination cathode materials. Moreover, many types of defects, especially heteroatoms and vacancies, have been introduced to enhance properties. It has been reported that the construction of hollow porous nanostructures by doping other atoms is a very effective strategy. Luo and colleagues reported a straightforward strategy to synthesize the composite of VO$_2$ and amorphous N-Doped carbon (VO$_2$@NC) via a simple calcination process.[83] The nanobelt structure can be observed in VO$_2$@NC, which has more active sites, higher conductivity and faster Zn^{2+} diffusion kinetics. The CV curves of the Zn/VO$_2$@NC cathode (Figure 7j) showed that it had excellent performance, possessing a remarkable capacity (435.4 mAh g^{-1} at 1.0 A g^{-1}) and a high retention rate of 96.3 % after 100 cycles at 1.0 A g^{-1}. Also, mixed valence vanadium oxides (e.g., V$_6$O$_{13}$) have been studied as potential materials. By doping Ni^{2+} to adjust the interlayer spacing of V$_6$O$_{13}$ crystals, Yuan with his collages obtained Ni-doped V$_6$O$_{13}$ (Ni$_x$V$_{6-x}$O$_{13}$) nanosheets.[84] The number of Ni precursors have a certain effort on the

Scheme 3. A main milestone history of Zn-based batteries.

Figure 7. a) The SEM image of the $Co_3V_2O_8@MnO_2$. b) The SEM image of the $V_2O_5\cdot4VO_2\cdot2.72H_2O$ nanobelts. c) The SEM image of the V–MOF nanorods. d) Schematic illustration of the synthesis of the $Co_3V_2O_8@MnO_2$. e) Projection of the framework along the a–axis showing 1D diamond–shaped channels. f) VO_6 chains cross-linked by 1, 4-benzenedicarboxylate (bdc). The differential charge density maps for g) $Ni_xV_{6-x}O_{13}$ and h) V_6O_{13} atomic layer slabs with the isosurface level of 0.03 e/Å³. In the differential density map, yellow region indicates electro accumulation. Red O, green V, and pink Ni atoms. i) CV curves of the Zn//nsutite–type VO_2 microcrystal battery at different scan rates. j) CV curves of the $VO_2@NC$ electrodes at various scan rates. k) CV curves of Zn// $Ni_{0.24}V_{5.76}O_{13}$ batteries at various scan rates. l) Schematic diagram for the electrochemical process of the as-obtained nsutite–type VO_2 microcrystal electrode. m) Various diffusion pathways of Zn ions among such $V_2O_5\cdot4VO_2\cdot2.72H_2O$ structures. Panels a and d: Reproduced with permission.[86] Copyright 2022, Elsevier. Panels b and m: Reproduced with permission.[85] Copyright 2021, Elsevier. Panels c, e, and f: Reproduced with permission.[87] Copyright 2021, Elsevier. Panels g, h, and k: Reproduced with permission.[84] Copyright 2022, Elsevier. Panels i and l: Reproduced with permission.[82] Copyright 2021, Elsevier. Panels j: Reproduced with permission.[83] Copyright 2022, Elsevier.

morphology and electrochemical performance of the $Ni_xV_{6-x}O_{13}$ nanosheets.

Interestingly, when Ni^{2+} ions are doped in the V_6O_{13} crystals, more charge carriers are transferred effectively to the conduction band of the layers (Figure 7g and h). As a result, the obtained electrode exhibited an excellent capacity of 302.6 mAh g^{-1} at 1.0 A g^{-1} and 96.5 mAh g^{-1} over 10,000 cycles at 8.0 A g^{-1} (Figure 7k). The porous structure of micro/nano MOFs endows electrode materials with new functions and properties, especially ultra–thin MOF nanosheets. For instance, Liu and colleagues used a simple hydrothermal approach to synthesize ultra–thin $V_2O_5\cdot4VO_2\cdot2.72H_2O$ nanosheets (Figure 7b) as cathode materials.[85] The formation of crystal water enlarges the interlayer spacing and shortens the diffusion path of Zn^{2+}. Schematic illustration of the reaction pathways in detail of Zn storage for the as–obtained layered $V_2O_5\cdot4VO_2\cdot2.72H_2O$ is presented in Figure 7m. The $V_2O_5\cdot4VO_2\cdot2.72H_2O$ cathode has a high capacity of 215 mAh g^{-1} at 0.1 A g^{-1}. At 10.0 A g^{-1}, 94.0% of the initial specific capacity was retained after 1000 cycles, and 85.2% was retained even after 2000 cycles. Moreover, the hollow nanostructured materials with large surface volume ratio, low density, special microreactor environment, high

loading capacity, and short charge transfer path have attracted wide attention. The unique hollow structure can usually provide a highly active region for electrochemical reactions, promoting mass transfer and ion diffusion. Zhang et al. adopted a simple hydrothermal method and in–situ growth strategy as shown in Figure 7d to obtain $Co_3V_2O_8@MnO_2$.[86] As can be additionally seen in Figure 7a, the surface of the $Co_3V_2O_8$ grows MnO_2 In–situ while the material becomes a hollow structure. The $Co_3V_2O_8@MnO_2$ cathode has a relatively high charging capacity of 245.4 mAh g^{-1} under 100 mA g^{-1}, which has ideal rate performance. When the current density is 300 mA g^{-1} after 300 cycles, the discharge capacity is about 140.0 mAh g^{-1}. Not only has high conductivity, but also can prevent excessive volume change. Therefore, the method of designing hollow nanostructures can be a reasonable way to manufacture high–performance water–based zinc ion battery cathodes. In addition, Ru with colleagues reported a new self–sacrificing approach to synthesis three–dimensional conductive vanadium–based MOFs (MIL-47) nanowire–bundle arrays on carbon nanotube fibers (Figure 7c).[87] Such specific configuration shown in Figure 7e, f provides abundant empty tunnels that are available for quick and efficient guest molecule transport.

Batteries & Supercaps

Review
doi.org/10.1002/batt.202400064

Chemistry Europe
European Chemical
Societies Publishing

Therefore, it can be inferred that the open framework of the V–MOF may accelerate the spread of Zn^{2+} ions in electrolyte. Due to rich active sites and layered porosity, the assembled ZIB offers a high capacity of 101.8 mAh cm^{-3} at a current density of 0.1 A cm^{-3}, and an excellent rate capability (64.3% of initial capacity after a 50-fold increase in current density). Interestingly, it has not only a high energy density of 17.4 mWh cm^{-3} but also a high–power density of 1.46 W cm^{-3}. Besides these, vanadium phosphates, vanadate, vanadium sulfides, VNs and so on can improve the electrochemical performance. Conductive MOFs (c-MOFs) have also been used in improving the performance of ZIBs.[88] C–MOFs have two mechanisms to transfer electrons, one is hopping transport, and the other is band transfer. For example, 1D c-MOF named Cu–BTA–H and 2D c-MOF called Ni–PTA–Mn can both increase the capacity and enhance the cycling stability of the ZIBs.

In addition, MXenes are another attractive material in ZIBs.[89,90] Lu with colleagues successfully used microfluidic–assisted 3D printing to prepare MXene/Cu–THBQ, which achieves stable Zn cycling and high reversible cycling.[91] Liu group reported NMO/MXene cathodes in ZIBs, outperforming most reported Mn–based electrodes.[92] These demonstrate the great potential of MXene for high performance ZIBs.

In conclusion, ZIBs have the great potential to drive the next generation of wearable electronic devices. The working mechanism is mainly from the matrix material insertion/extraction of Zn^{2+}. Most research focuses on the use of V-based materials (V (III), V (IV), V (V)) to prepare the cathodes. Most layered V-based compounds are composed of VO_x layers, which are prone to irreversible phase transitions and structural collapse during Zn^{2+} (de)intercalation, thus limiting cycling stability. To further improve the performance of ZIBs, it is a promising strategy to construct porous structures, and hollow nanostructures, or improve the synthesis process and incorporate heteroatoms.

3. Supercapacitors

In recent decades, the demand for efficient and convenient electrochemical energy storage has been increasing. In addition to the previously mentioned batteries, supercapacitors (SCs) are another promising means of energy storage,[93] which show great promise in many fields including digital cameras, electric hybrid vehicles, and energy storage, especially in wearable electronics applications.[94] It has the characteristics of long–life cycle, wide voltage range and high coulomb efficiency.[95,96] According to the charge storage mechanism, SCs can be mainly divided into two types: electric double–layer capacitors (EDLCs) and pseudo–capacitors. EDLCs store electrical energy in the form of static electricity. Expanding the surface area is essential for enhancing the electrochemical performance of layer capacitors, as it enables the acquisition of electrolytes.[97] Many carbon–based materials have been developed as electrode materials for EDLCs.[98] However, EDLCs show relatively low energy density and capacitance. Pseudo–capacitors are based on reversible REDOX reactions between electrodes and electrolytes. Lots of cheap TMOs and various precious metals are used such as Co_3O_4, Fe_2O_3, and $NiCo_2O_4$.[99] The overall performance of SCs is highly dependent on the inherent properties of the electrode material. Therefore, one of the most difficult challenges is the selection of electrode materials. At present, nano MOFs have been deeply studied for SCs. (Table 3)

3.1. MOF/Carbonaceous Materials

Carbonaceous materials are potential electrode materials for EDLCs. Expanding their surface area can further enhance the performance of the electrode. Thus, MOF/carbonaceous composites and their derivatives with high surface areas are prospective. Graphene oxide and reduced graphene oxide (GO and rGO) with their unique layered structures have excellent ion diffusion and transportation ability when combined with nano MOFs. The Zhou group prepared a series of Ni–MOFs and Ni–MOFs@GO via a simple hydrothermal method.[107] The obtained Ni–MOFs@3 wt% GO electrode displayed a superior capacitance of 2192.4 F g^{-1} at 1 A g^{-1} and outstanding cycling endurance of 85.1% capacitance retention even after 3000 cycles. The direct mixing process is also a common method. Also, the Saraf group obtained a Cu–MOF/rGO hybrid and modified glassy carbon electrodes.[41] Cu–MOF and rGO powder were dispersed in ethanol, followed by ultrasonication. The final product was obtained after rotary evaporation and washing by ethanol and deionized water. The synergistic effect between the MOF and rGO enhanced the electrical conductivity and minimized the internal resistance. Doping is another pretty effective strategy. For instance, Banerjee and colleagues obtained a composite of Ni–doped MOF with rGO.[108] The highly effective charge transfer process was likely due to the coordination function of the distributed Ni centers in the MOF-5 (Ni50% rGO50%) and interconnected graphene nanosheets. MOF-5 electrode demonstrated a superior energy density of 37.8 Wh kg^{-1} at 226.7 W kg^{-1} and displayed an attractive stability during the cycling process. Meanwhile, Wang and co–workers prepared 3D Co–doped Ni–based MOFs flower-like hierarchical microspheres (Co_x–Ni–MOF).[109] This product en-

Table 3. MOF, MOF composites and their derivatives for SCs electrode materials.

Electrode materials	Specific capacitance (F g^{-1})	Current density (mA g^{-1})	Power density (W kg^{-1})	Ref.
Fe–Co–S/NF	2695	1000.0	770.0	[68]
$Li_4Ti_5O_{12}$/NGO	73.56	1000.0	799.8	[99]
ZIF-8@ZIF-67	270.0	5000.0	–	[100]
$Co_2V_2O_7 \cdot nH_2O$	271.9	10000	745.1	[101]
Co_3O_4/CoC_2O_4	44.60	500.00	550.7	[102]
CoMOF@Ni/C	37.49	500.00	–	[103]
Co–MOF NS	1159	500.00	–	[104]
Ni–HHTP@Ni(OH)$_2$	79.80	500.00	375.0	[105]
MnO_2@Ni-HHTP	368.2	1000.0	3000	[106]

Batteries & Supercaps

Review
doi.org/10.1002/batt.202400064

Chemistry Europe
European Chemical
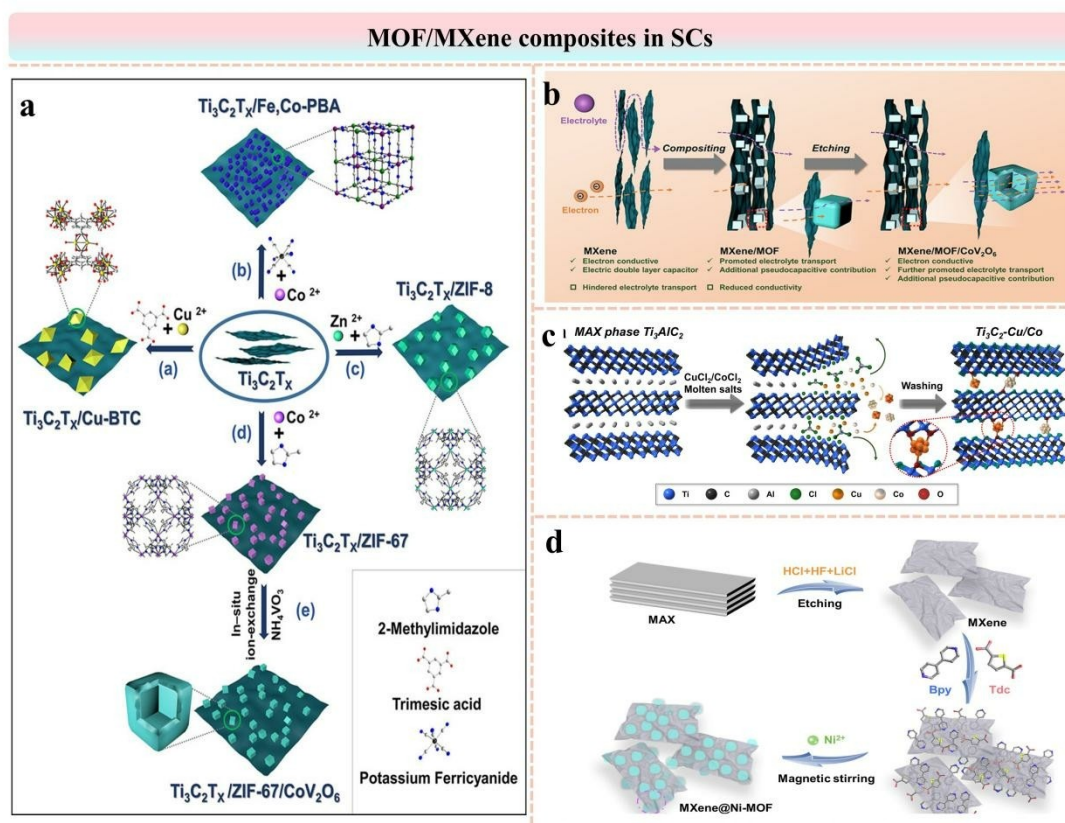Societies Publishing

joyed a more open hierarchical structure due to Co doping, which contributed to contact between active sites and electrolyte ions. Moreover, part of Ni^{2+} was replaced by Co^{2+} in Co_x–Ni–MOF, producing more "free holes" and further improving the conductivity. The obtained Co_2–Ni–MOF exhibited a superior specific capacitance of 1300 F g^{-1} at 1 A g^{-1} and an excellent rate performance of 1021 F g^{-1} at 10 A g^{-1}.

In conclusion, the combination of graphene–based materials and MOFs is undoubtedly an effective strategy to provide suitable electrode materials for supercapacitors. The low capacitance and electron mobility of traditional MOF–based SCs prevent their electrodes from displaying their optimal performance. In contrast, the assembly of graphene–based materials and MOFs overcomes these shortcomings, bringing better capabilities to the mixing material. At present, the main strategies are focused on direct preparation, solvothermal method, in–situ growth method, etc., using GO, rGO and other graphene–based materials to prepare higher performance electrode materials.

3.2. MOF/MXene Composite Materials

MXenes are one of the most important materials reported in 2D nanomaterials. The energy storage mechanism of MXenes mainly belongs to EDLCs. Their combinations with MOF have great potential in avoiding the accumulation of MXene nanosheets and facilitating the transport of electrolytes. The most common MXene/MOF systems are $Ti_3C_2T_x$/Fe, $Ti_3C_2T_x$/ZIF-8, and $Ti_3C_2T_x$/ZIF-67. To improve the electrochemical performance, the basic research is to introduce new metal ions or construct hollow porous structures on this basis. For example, Liu and co-workers obtained $Ti_3C_2T_x$/ZIF-67 by co–precipitation reaction and prepared hollow $Ti_3C_2T_x$/ZIF-67/CoV_2O_6 composite via an "ion conversion–exchange" strategy[110] (Figure 8a). The electrolyte/electron transport in $Ti_3C_2T_x$, $Ti_3C_2T_x$/ZIF-67 and hollow $Ti_3C_2T_x$/ZIF-67/CoV_2O_6 is shown in Figure 8b. The composites demonstrate a desirable capacitance of 253.8 F g^{-1} at 5 A g^{-1}. In addition, MXene@ZIF-67/core–shell/yolk–shell cobalt hydroxide (MXene@CS–ZCH/MXene@YS–ZCH) and hollow cobalt hydroxide (MXene@Ho–CH) composites were prepared by in–situ gradient etching.[111] It provides a strategy to achieve MXene synthesis with layered core–shell/yolk/shell/hollow structures of MOF derivatives. Of all the MXenes discovered, the most extensively studied is Ti_3AlC_2, which is usually synthesized by etching method. To find a harmless and cleaner strategy and improve the energy storage performance, Lewis's acid molten salt etching method was proposed. Liu and colleagues report the preparation of etching Ti_3C_2–Cu/Co hybrid Lewis's acid melt salt.[112] Lewis's acid non–precious metal elements copper and

Figure 8. a) Schematic illustration of the synthesis of $Ti_3C_2T_x$/Cu–BTC, $Ti_3C_2T_x$/Fe, Co–PBA, $Ti_3C_2T_x$/ZIF-8, $Ti_3C_2T_x$/ZIF-67, and $Ti_3C_2T_x$/ZIF-67/CoV_2O_6. b) Schematic diagram for electrolyte/electron transport in $Ti_3C_2T_x$, $Ti_3C_2T_x$/ZIF-67 and hollow $Ti_3C_2T_x$/ZIF-67/CoV_2O_6. c) Preparation of Ti_3C_2–Cu/Co hybrids. d) Preparation of MXene@Ni–MOF. Panels a and b: Reproduced with permission.[110] Copyright 2022, Wiley. Panels c: Reproduced with permission.[112] Copyright 2021, Wiley. Panels d: Reproduced with permission.[113] Copyright 2022, Elsevier.

Batteries & Supercaps

Review

doi.org/10.1002/batt.202400064

Chemistry
Europe

European Chemical
Societies Publishing

cobalt play a crucial role in conversion processes because of their polyvalent states and catalytic activity. Ti_3C_2–Cu and Ti_3C_2–Co were obtained by etching Ti_3AlC_2 with molten copper or cobalt chloride (Figure 8c). A supercapacitor was prepared using Ti_3C_2–Cu as electrode and sulfuric acid as electrolyte. The symmetric supercapacitor Ti_3C_2–Cu//Ti_3C_2–Cu has an area capacitance of 290.5 mF cm^{-2} at 1 mA cm^{-2}. This unique insertion structure, and the synergistic effect of Ti_3C_2 and Cu provide a new strategy for molten salt method and active material design based on diene–metal hybrid. In addition, according to reports, the strong interaction between Ni–MOF organic ligand and MXene surface functional groups can not only reduce the exposure of MXene surface functional groups, limit its oxidation, but also increase its layer spacing and promote the rapid transfer of ions. These advantages make the combination of Ni–MOF and MXene play a key role in the application of SCs. Inspired by this, Zhou with colleagues reportedMXene@pillared–layer MOF composites (MXene@Ni–MOF)[113] and the main formation process is shown here in Figure 8d. The product uses MXene to fix Ni–MOF nanosheets to realize rapid charge transfer, thus solving the problem of poor Ni–MOF conductivity and realizing high cycle stability. The MXene@Ni–MOF exhibits a high specific capacitance of 979 F g^{-1} at 0.5 A g^{-1} and have enhanced electrical properties and higher electrochemical properties than the original Ni–MOFs. To design an outstanding REDOX activity and attractive stability supercapacitor, bimetallic MOFs and aminated MOF are combined to synthesis and assemble Ni/Co–MOF@$Ti_3C_2T_x$–NH$_2$. The reason for the rapid REDOX reaction is roughly the presence of a highly conductive MXene network, which produces sufficient Ni and Co REDOX active substances.
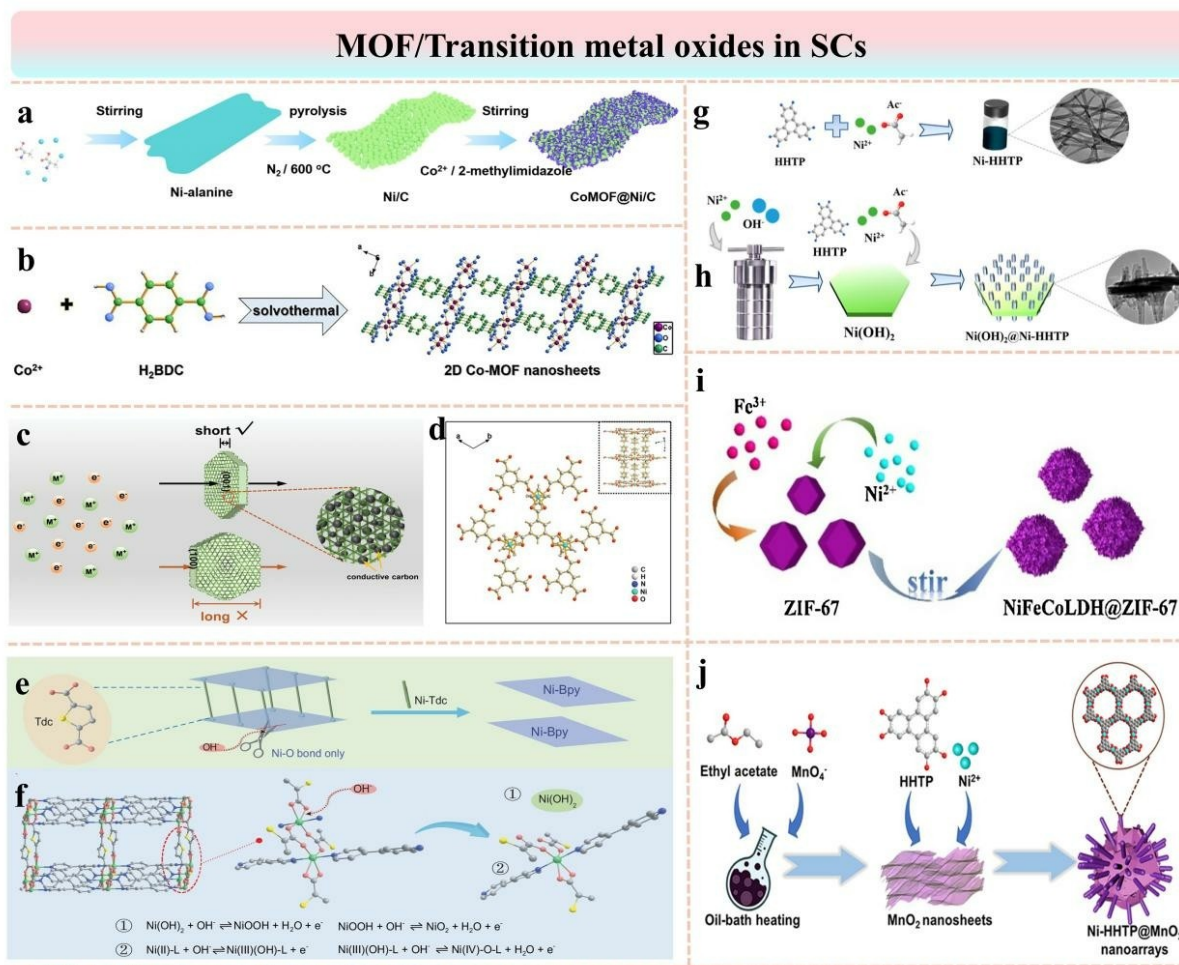
In short, MOF/MXene composites have achieved many attractive and superior electrochemical properties. Meanwhile, lots of MOF–derived materials have been successfully designed and applied in SCs, such as metal oxides, metal phosphates, and metal selenides. These materials with reasonable structures and clever designs have obvious layered structure, larger active area, and layer spacing, which can effectively achieve the rapid electrons/ions transfer.

3.3. MOF/Transition Metals and Their Oxides (TMOs)

Transition metal oxides applied in SCs have been extensively studied in recent decades. Ru–based materials, including RuO_2, RuO and Ru composites, are rare, multivalent, and multi–functional materials with strong corrosion resistance.[114] Thus, people study Co–MOF, Ni–MOF, and Mn–MOF.[115] Primitive Co–MOF has attracted much attention. To further improve its conductivity, Wang and colleagues came up with the idea of using MOFs in situ immobilization,[103] which is in–situ growth on Ni/C precursors through Co–MOF as shown in Figure 9a. It effectively prevents excessive aggregation of Ni nanoparticles in Ni/C precursors and expands the contact area of the electrolyte, thereby promoting mass and electron transfer. Thereinto, CoMOF@Ni/C with a stirring duration of 12 h (denoted as F-12) demonstrated a maximal specific capacitance of 27.73 mAh g^{-1}.

The F-12//AC aqueous device was created with a cycling feature that only showed 8% decay. MOF–derived Co_3O_4 is also outstanding and favored, but the researchers observed its limitations, such as low ion diffusivity and drastic volume expansion. Adding conductive substrates, especially graphene and carbon cloth, is a useful and prospective method. Yin and co–workers first annealed Co–MOF on a carbon cloth to make the derived cobalt oxide, which they then combined with NiCo–LDH to build a hybrid Co_3O_4@NiCoLDH. The materials provide a high energy density of 44.44 Wh kg^{-1} at the power density of 0.80 kW kg^{-1}. In addition, the structure of nano materials plays a vital part in the performance. In comparison, low–dimensional materials are prone to agglomeration and their applications are limited.[100] While 2D and 3D materials composed of different structure units have exhibited excellent performance.[101] They can facilitate sufficient contact with electrolyte, ensure fast intercalation of ions, and rapid charge transfer. Zheng group reported ultrathin 2D Co–MOF nano-sheets [$Co_2(OH)_2$BDC, BDC=1,4-benzenedicarboxylate][104] as shown in (Figure 9b). The as–prepared electrode successfully displayed an ultra–high capacitance of 1159 F g^{-1} at 0.5 A g^{-1}. The results show that better nanostructures demonstrate higher specific capacitance and have greater potential to be desirable supercapacitor electrode. Meanwhile, nickel–based materials have always been regarded as strong competitors.[116] But the structure stability, rate capability, and cycle life are poor during the fast charge and discharge process. Thus, the design and synthesis of stable size/morphology–controlled MOF nanocrystals are critical but challenging. Xu et al. prepared [Ni$(NO_3)_2\cdot6H_2O$, 1,3,5-benzenetricarboxylic acid, 4,4′-bipyridine].[117] Figure 9d is a view of the 3D porous structures along the *ab*-axis. As shown in Figure 9c, the transportation path is shortened, and the transportation rate is accelerated. Dual–ligand and hard–soft–acid–base strategies were used by Sun and co–workers to fabricate 3D pillared–layer MOF nanocrystal with controllable morphology by varying the concentration of 4,4-bipyridine and thus, controlling the crystal growth direction.[118] The main mechanism of charge/discharge is shown here in Figure 9e and f. Owing to the shorter ion diffusion length and enhanced electron/ion transfer, the 2D nanosheets showed much larger specific capacitance than the 1D nano-fibers and 3D aggregates. Exceptional cycling performance (95% of retention after 5000 cycles at 3 mA cm^{-2}) was realized by configuring two aqueous asymmetric supercapacitor devices in series. In addition, the design of c-MOF composites is another meaningful method.[119] Duan successfully[105] designed and combined a typical conductive MOF Ni–HHTP and a serious of Ni–HHTP@Ni$(OH)_2$ nanoarrays (Figure 9g and h). An assembled aqueous supercapacitor demonstrated an excellent cycling stability with 98% of the original capacitance remained. More-over, Zhao et al. successfully synthesized a series of MnO_2@Ni–HHTP[106] as shown in Figure 9j. Owing to the REDOX activity of MnO_2 and the desirable conductivity in Ni–HHTP, the cathode materials can reach high energy density, good rate performance and excellent cycle stability in SCs. In addition, the introduction of secondary metal ions, especially Co^{2+}, can not only stabilize nickel, but also provide more active sites and

Batteries & Supercaps

Review
doi.org/10.1002/batt.202400064

Chemistry Europe
European Chemical
Societies Publishing

Figure 9. a) The formation diagram of CoMOF@Ni/C. b) Preparation of ultrathin 2D Co–MOF NS. c) Schematic diagram for charge transfer process on (001) and rectangular crystal planes. d) View of structures of hexagonal Ni–MOF 2D layer along the *ab*-axis. Over the upper right corner, a view of the structure perpendicular to the 2D layer. e) Schematic for the selective removal of Tdc carboxylate links from [Ni (Tdc)(Bpy)] $_n$ nanosheets by OH-in the electrolyte during charging and discharging. f) Mechanism of charge/discharge of a [Ni (Tdc)(Bpy)] $_n$ MOF–based electrode. g) Schematic diagram for the synthesis of Ni–HHTP nanoarrays. h) Schematic illustration of the preparation of Ni (OH)$_2$@Ni–HHTP nanoarrays. i) The synthesis diagram of NiCoFeLDH@ZIF-67. j) The formation illustration of MnO$_2$@NiHHTP nanoarrays. Panels a: Reproduced with permission.[103] Copyright 2022, Elsevier. Panels b: Reproduced with permission.[104] Copyright 2019, Elsevier. Panels c and d: Reproduced with permission.[117] Copyright 2019, Wiley. Panels e and f: Reproduced with permission.[118] Copyright 2022, Oxford University Press. Panels g and h: Reproduced with permission.[105] Copyright 2022, American Chemical Society. Panels i: Reproduced with permission.[107] Copyright 2021, Elsevier. Panels j: Reproduced with permission.[106] Copyright 2021, American Chemical Society.

improve its conductivity. Therefore, the preparation of Co/Ni–MOF materials is an effective method to improve the performance of SCs. Zhao et al. used Ni–MOF ([Ni$_3$(OH)$_2$(TDC)$_2$(H$_2$O)$_4$] $_n$, H$_2$TDC $=$ 2, 5-thienobenzoic carboxylic acid) as a prototype model and introduced Co^{2+} to obtain Co/Ni–MOF,[119] which can effectively regulate its inherent reactivity and conductivity. It exhibited a maximum specific capacitance of 228 F g^{-1} at 0.5 A g^{-1}, a capacity retention rate of 68% at 5 A g^{-1} and maintains 95.5% capacitance after 5000 cycles. The synergistic effect of Ni^{2+} and Co^{2+} can not only improve the conductivity, but also provide more active sites to promote ion and electron transfer. In addition, Shan obtains Ni–Co–MOF by calcination of composite materials,[121] which provides an attractive idea via designing rationally the heteroatom–doped ZIF-67. The product can accelerate electron transfer and further promote electrolyte diffusion. Co/Mn–ZIF cube was prepared by Shi via a simple one–step coprecipitation method.[122] Due to

the doping of manganese ions, the final product has a good structure, higher surface area and satisfactory electrochemical conductivity. Co/Mn–ZIF-based materials also had a remarkable capacitance of 926.25 F g^{-1} at a current density of 0.5 A g^{-1}. It has been reported that materials with distinct layers of hollow micro–nano structures usually show interesting sequential organization of pores and pores, which have a non–negligible effect on the occurrence of synergies. So far, people have been focusing on the development of hollow structure materials to for flexible solid–state SCs. Therefore, layered porous nano-structures can be constructed to improve its performance. Cao's group obtained a multi–component hierarchical structure by growing NiCoFeLDH on the surface of ZIF-67.[107] Figure 9i exhibited the synthesis diagram of NiCoFeLDH@ZIF-67. The hydrolysis acidity of metal ions and the coordination ability with ligands were the key factors for forming this nanosheets and hollow structures. The hollow NiCoFeLDH@ZIF-67 compo-

Batteries & Supercaps

Review
doi.org/10.1002/batt.202400064

Chemistry Europe
European Chemical
Societies Publishing

site can reach a specific capacitance of 1202.08 F g^{-1} at 0.5 A g^{-1}.

To conclude, at present, MOF/TMOs for SCs are mainly Co–MOF, Ni–MOF, and polymetallic MOF. Most cobalt–based and nickel–based materials with broad practical application prospects have much larger specific capacitors than others. At the same time, compared with ordinary nanostructured TMOs, layered nanostructured and hollow–core–shell isomerized TMOs have higher specific capacitance and better cycle performance. However, while this nanostructure facilitates the electrochemical reaction of TMO electrode materials, this structure often results in a low tap density. Thus, a new rational structure should be designed to withstand the large volume energy density. The application of TMOs in asymmetric SCs is a hot spot, which can combine various negative and positive materials with good separation potential to maximize the output voltage and has a wide application prospect.

4. Summary and Outlook

This paper reviews the recent applications of nano MOFs in energy storage, including different types of batteries and supercapacitors. Nano MOFs are promising and prospective materials for energy storage applications. Nevertheless, some challenges in practical applications remain: the high cost of ligands and MOF precursors, cumbersome fabrication processes, the inability to monitor structural pores in real time, higher demand for performance and so on. To overcome the short-comings mentioned above, we offer our views on how to address these issues. Reasonably select metal ions, organic ligands, and functional materials with multiple active sites and small molecular weight. Optimize the synthesis strategy. Strengthen the development and research of new nano MOFs. Understand the working mechanism. These can be beneficial to gain a more particular knowledge of MOF composites and derived materials, which is of great significance to guide subsequent exploration.

Acknowledgements

Conflict of Interests

The authors declare no conflict of interest.

[1] X. Guo, S. Wang, B. Yang, Y. Xu, Y. Liu, H. Pang, *J. Colloid Interface Sci.* **2020**, *561*, 801–807.
[2] X. Li, X. Yang, H. Xue, H. Pang, Q. Xu, *EnergyChem* **2020**, *2*, 100027.
[3] J. Shao, X. Li, J. Wei, H. Pang, C. Chen, *Adv. Sustainable Syst.* **2018**, *2*, 1700154.
[4] W. Du, R. Kang, P. Geng, X. Xiong, D. Li, Q. Tian, H. Pang, *Mater. Chem. Phys.* **2015**, *165*, 207–214.
[5] H. Zhou, S. Zheng, X. Guo, Y. Gao, H. Li, H. Pang, *J. Colloid Interface Sci.* **2022**, *628*, 24–32.
[6] Q. Li, Y. Xu, S. Zheng, X. Guo, H. Xue, H. Pang, *Small* **2018**, *14*, e1800426.
[7] H. Pang, Y. Zhang, Z. Run, W. Lai, W. Huang, *Nano Energy* **2015**, *17*, 339–347.
[8] Y. Tang, S. Zheng, S. Cao, F. Yang, X. Guo, S. Zhang, H. Xue, H. Pang, *J. Colloid Interface Sci.* **2022**, *626*, 1062–1069.
[9] J. Ma, X. Guo, Y. Yan, H. Xue, H. Pang, *Adv. Sci.* **2018**, *5*, 1700986.
[10] Y. Gao, X. Guo, Z. Qiu, G. Zhang, R. Zhu, Y. Zhang, H. Pang, *ChemPhysMater* **2022**, *1*, 17–38.
[11] L. Zhang, S. Zheng, L. Wang, H. Tang, H. Xue, G. Wang, H. Pang, *Small* **2017**, *13*, 1700917.
[12] Y. Zhang, J. Zhao, J. Xia, L. Wang, W. Y. Lai, H. Pang, W. Huang, *Sci. Rep.* **2015**, *5*, 8536.
[13] H. Zhou, H. Yang, S. Yao, L. Jiang, N. Sun, H. Pang, *Chin. Chem. Lett.* **2022**, *33*, 3681–3694.
[14] P. Zhu, X. Li, H. Yao, H. Pang, *J. Energy Storage* **2020**, *31*, 101544.
[15] Q. Li, Y. Zhang, G. Zhang, Y. Wang, H. Pang, *Natl. Sci. Open* **2023**, *2*, 20220065.
[16] J. Xu, J. Ma, Y. Peng, S. Cao, S. Zhang, H. Pang, *Chin. Chem. Lett.* **2023**, *34*, 107527.
[17] J. Ding, Y. Tang, S. Zheng, S. Zhang, H. Xue, Q. Kong, H. Pang, *Nano Res.* **2022**, *15*, 6793–6818.
[18] H. Yang, H. Zhou, G. Zhang, X. Guo, H. Pang, *Sci. China Mater.* **2022**, *66*, 441–469.
[19] Q. Li, S. Zheng, M. Du, H. Pang, *Chem. Eng. J.* **2021**, *417*, 129201.
[20] Y. Xue, X. Hang, J. Ding, B. Li, R. Zhu, H. Pang, Qiang Xu, *Coord. Chem. Rev.* **2021**, *430*, 213656.
[21] M. Zhao, Q. Zhao, J. Qiu, X. Lu, G. Zhang, H. Xue, H. Pang, *Part. Part. Syst. Charact.* **2017**, *34*, 1600412.
[22] S. Zheng, Q. Li, H. Xue, H. Pang, Q. Xu, *Natl. Sci. Rev.* **2020**, *7*, 305–314.
[23] C. Liu, J. Li, H. Pang, *Coord. Chem. Rev.* **2020**, *410*, 213222.
[24] X. Wang, G. Zhang, W. Yin, S. Zheng, Q. Kong, J. Tian, H. Pang, *Carbon Energy.* **2022**, *4*, 246–281.
[25] X. Tang, N. Li, H. Pang, *Green Energy & Environ.* **2022**, *7*, 636–661.
[26] Y. Shi, B. Zhu, X. Guo, W. Li, W. Ma, X. Wu, H. Pang, *Energy Storage Mater.* **2022**, *51*, 840–872.
[27] Y. Li, Y. Xu, W. Yang, W. Shen, H. Xue, H. Pang, *Small* **2018**, *14*, e1704435.
[28] Y. Qian, F. Zhang, S. Zhao, C. Bian, H. Mao, D. Kang, H. Pang, *Nano Energy* **2023**, *111*, 108415.
[29] D. Zhou, X. Guo, Q. Zhang, Y. Shi, H. Zhang, C. Yu, H. Pang, *Adv. Funct. Mater.* **2021**, *32*, 2107928.
[30] W. Hu, M. Zheng, B. Xu, Y. Wei, W. Zhu, Q. Li, H. Pang, *J. Mater. Chem. A* **2021**, *9*, 3880–3917.
[31] X. Guo, W. Li, P. Geng, Q. Zhang, H. Pang, Q. Xu J Colloid, *Interface Sci.* **2022**, *606*, 784–792.
[32] Y. Cheng, X. Xiao, K. Pan, H. Pang, *Chem. Eng. J.* **2020**, *380*, 122565.
[33] W. Yin, G. Zhang, X. Wang, H. Pang, *Adv. Colloid Interface Sci.* **2021**, *298*, 102562.
[34] H. Zhou, X. Li, Y. Li, M. Zheng, H. Pang, *Nano-Micro Lett.* **2019**, *11*, 40.
[35] G. Song, Y. Shi, J. Jiang, H. Pang, *Adv. Funct. Mater.* **2023**, e2303121.
[36] C. Wang, X. Li, Q. Li, H. Pang, *FlatChem* **2019**, *16*, 100107.
[37] Y. Peng, J. Xu, J. Xu, J. Ma, Y. Bai, S. Cao, S. Zhang, H. Pang, *Adv. Colloid Interface Sci.* **2022**, *307*, 102732.
[38] J. Xu, Y. Peng, W. Xing, Z. Ding, S. Zhang, H. Pang, *J. Energy Storage* **2022**, *53*, 105104.
[39] L. Chen, X. Guo, W. Lu, M. Chen, Q. Li, H. Xue, H. Pang, *Coord. Chem. Rev.* **2018**, *368*, 13–34.
[40] X. Zhang, S. Zhang, Y. Tang, X. Huang, H. Pang, *Composites Part B* **2022**, *230*, 109532.
[41] Y. Zheng, S. Zheng, H. Xue, H. Pang, *Adv. Funct. Mater.* **2018**, *28*, 1804950.

Batteries & Supercaps

Review

doi.org/10.1002/batt.202400064

Chemistry
Europe

European Chemical
Societies Publishing

[42] B. Li, P. Gu, G. Zhang, Y. Lu, K. Huang, H. Xue, H. Pang, *Small* **2018**, *14*, 1702184.

[43] S. S. Jan, S. Nurgul, X. Shi, H. Xia, H. Pang, *Electrochim. Acta.* **2014**,*149*, 86–93.

[44] J. Wang, N. Li, Y. Xu, H. Pang, *Chem. Eur. J.* **2020**, *26*, 6402–6422.

[45] Z. Yang, S. Cao, T. Lv, G. Zhang, X. Guo, S. Zhang, H. Pang, *MRS Energy Sustainability* **2022**, *9*, 281–312.

[46] Z. Meng, Z. Qiu, Y. Shi, S. Wang, G. Zhang, Y. Pi, H. Pang, *eScience* **2023**, *3*, 1000092.

[47] Y. Shi, G. Zhu, X. Guo, Q. Jing, H. Pang, Y. Zhang, *Nano Res.* **2022**, *16*, 2528–2535.

[48] H. Yang, G. Zhang, H. Zhou, Y. Sun, H. Pang, *Energy Mater. Adv.* **2023**, *4*, 0033.

[49] Z. Qiu, Y. Bai, Y. Gao, C. Liu, Y. Ru, Y. Pi, Y. Zhang, Y. Luo, H. Pang, *Rare Met.* **2021**, *41*, 1101–1128.

[50] H. Pang, Z. Yan, Y. Ma, G. Li, J. Chen, J. Zhang, W. Du, S. Li J, *Solid-State Electron.* **2013**, *17*, 1383–1391.

[51] J. Ma, X. Guo, H. Xue, K. Pan, C. Liu, H. Pang, *Chem. Eng. J.* **2020**, *380*, 122428.

[52] Y. Shan, M. Zhang, Y. Bai, M. Du, X. Guo, H. Pang, *Chem. Eng. J.* **2022**, *429*, 132146.

[53] Y. Shi, X. Pan, B. Li, M. Zhao, H. Pang, *Chem. Eng. J.* **2018**, *343*, 427–446.

[54] Y. Hua, X. Li, C. Chen, H. Pang, *Chem. Eng. J.* **2019**, *370*, 37–59.

[55] N. Li, Q. Li, X. Guo, M. Yuan, H. Pang, *Chem. Eng. J.* **2019**, *372*, 551–571.

[56] X. Guo, C. Chen, Y. Zhang, Y. Xu, H. Pang, *Energy Storage Mater.* **2019**, *23*, 439–465.

[57] F. Wang, J. Hu, Y. Peng, X. Wu, H. Xue, H. Pang, *ASEM* **2023**, *2*, 100053.

[58] M. Du, Q. Li, H. Pang, *J. Colloid Interface Sci.* **2020**, *580*, 614–622.

[59] M. Zheng, H. Tang, L. Li, Q. Hu, L. Zhang, H. Xue, H. Pang, *Adv. Sci.* **2018**, *5*, 1700592.

[60] X. Xiao, L. Zou, H. Pang, Q. Xu, *Chem. Soc. Rev.* **2020**, *49*, 301–331.

[61] W. Zhou, Y. Tang, X. Zhang, S. Zhang, H. Xue, H. Pang, *Coord. Chem. Rev.* **2023**, *477*, 214949.

[62] J. Wang, Q. Hu, W. Hu, W. Zhu, Y. Wei, K. Pan, M. Zheng, H. Pang, *Molecules* **2022**, *27*, 396.

[63] Y. Wei, M. Zheng, W. Zhu, H. Pang, *Carbon Neutralization.* **2023**, *2*, 271–299.

[64] X. Wu, Y. Ru, Y. Bai, G. Zhang, Y. Shi, H. Pang, *Coord. Chem. Rev.* **2022**, *451*.

[65] Y. Xu, S. Zheng, H. Tang, X. Guo, H. Xue, H. Pang, *Energy Storage Mater.* **2017**, *9*, 11–30.

[66] L. Fan, X. Guo, X. Hang, H. Pang, *J. Colloid Interface Sci.* **2022**, *607*, 1898–1907.

[67] S. Yang, Y. Cheng, X. Xiao, H. Pang, *Chem. Eng. J.* **2020**, *384*, 123294.

[68] L. Jiang, H. Zhou, H. Yang, N. Sun, Z. Huang, H. Pang, *J. Energy Storage* **2022**, *55*, 105354.

[69] M. Du, Q. Li, Y. Zhao, C. Liu, H. Pang, *Coord. Chem. Rev.* **2020**, *416*, 213341.

[70] M. Zheng, Y. Chi, Q. Hu, H. Tang, X. Jiang, L. Zhang, S. Zhang, H. Pang, Q. Xu J Mater, *Chem. A* **2019**, *7*, 17204–17241.

[71] M. Du, X. Wang, P. Geng, Q. Li, Y. Gu, Y. An, H. Pang, *Chem. Eng. J.* **2021**, *420*, 130518.

[72] M. Du, P. Geng, C. Pei, X. Jiang, Y. Shan, W. Hu, L. Ni, H. Pang, *Angew. Chem. Int. Ed.* **2022**, *61*, e202209350.

[73] P. Geng, L. Wang, M. Du, Y. Bai, W. Li, Y. Liu, S. Chen, P. Braunstein, Q. Xu, H. Pang, *Adv. Mater.* **2022**, *34*, e2107836.

[74] P. Geng, M. Du, X. Guo, H. Pang, Z. Tian, P. Braunstein, Q. Xu, *Energy Environ. Mater.* **2021**, *5*, 599–607.

[75] W. Li, X. Guo, P. Geng, M. Du, Q. Jing, X. Chen, G. Zhang, H. Lu, Q. Xu, P. Braunstein, et al., *Adv. Mater.* **2021**, *33*, e2105163.

[76] Y. Ru, S. Zheng, H. Xue, H. Pang, *Mater. Today Chem.* **2021**, *21*, 100513.

[77] L. Fan, Y. Ru, H. Xue, H. Pang, Q. Xu, *Adv. Sustainable Syst.* **2020**, *4*, 2000178.

[78] L. Kong, M. Cheng, H. Huang, J. Pang, S. Liu, Y. Xu, X. Bu, *EnergyChem* **2022**, *4*, 100090.

[79] T. Huang, M. Cheng, Y. Yuan, L. Kong, Z. Chang, X. Bu, *Dalton Trans.* **2023**, *52*, 13737.

[80] H. Tian, Y. Zhang, D. Yu, X. Yang, H. Wang, C. Matindi, Z. Yin, H. Hui, B. Mamba, J. Li, *Electrochim. Acta.* **2022**, *426*, 140796.

[81] T. Lv, Y. Peng, G. Zhang, S. Jiang, Z. Yang, S. Cao, H. Pang, *Adv. Sci.* **2023**, *10*, e2206907.

[82] Y. Liu, T. Lv, H. Wang, X. Guo, C. Liu, H. Pang, *Chem. Eng. J.* **2021**, *417*, 128408.

[83] T. Lv, X. Luo, G. Yuan, S. Yang, H. Pang, *Chem. Eng. J.* **2022**, *428*, 131211.

[84] Y. Liu, G. Yuan, X. Wang, J. Liu, Q. Zeng, X. Guo, H. Wang, C. Liu, H. Pang, *Chem. Eng. J.* **2022**, *428*, 132538.

[85] T. Lv, Y. Liu, H. Wang, S. Yang, C. Liu, H. Pang, *Chem. Eng. J.* **2021**, *411*, 128533.

[86] T. Lv, G. Zhang, Sh. Zheng, X. Guo, T. Chen, Sh. Yang, H. Pang, *Chem. Eng. J.* **2022**, *440*, 135931.

[87] B. He, Q. Zhang, P. Man, Z. Zhou, C. Li, Q. Li, L. Xie, X. Wang, H. Pang, Y. Yao, *Nano Energy* **2019**, *64*,103935.

[88] Q. Zhang, S. Jiang, T. Lv, Y. Peng, H. Pang, *Adv. Mater.* **2023**, e2305532.

[89] Y. Shen, H. Lv, L. Chen, *Mater. Chem. Front.* **2023**, *7*, 2373.

[90] M. Javed, A. Mateen, S. Ali, X. Zhang, I. Hussain, M. Imran, S. Shah, W. Han, *Small* **2022**, *18*, 2201989.

[91] H. Lu, J. Hu, K. Zhang, J. Zhao, S. Deng, Y. Li, B. Xu, H. Pang, *Adv. Mater.* **2024**, *36*, 2309753.

[92] Y. Liu, Y. Mei, W. Xu, M. Zhang, J. Hou, Y. Dong, *J. Alloys Compd.* **2023**, *957*, 170397.

[93] J. Zhao, M. Zheng, Z. Run, J. Xia, M. Sun, H. Pang, *J. Power Sources* **2015**, *285*, 385–392.

[94] Y. Zhang, M. Zheng, M. Qu, M. Sun, H. Pang, *J. Alloys Compd.* **2015**, *651*, 214–221.

[95] W. Du, Z. Zhu, Y. Xu, Z. Zhang, X. Xiong, P. Geng, H. Pang, *J. Solid State Electrochem.* **2015**, *19*, 2177–2188.

[96] J. Zhao, S. Wang, Z. Run, G. Zhang, W. Du, H. Pang, *Part. Part. Syst. Charact.* **2015**, *32*, 880–885.

[97] M. Zheng, X. Xiao, L. Li, P. Gu, X. Dai, H. Tang, Q. Hu, H. Xue, H. Pang, *Sci. China Mater.* **2017**, *61*, 185–209.

[98] H. Pang, Y. Zhang, W. Lai, Z. Hu, W. Huang, *Nano Energy* **2015**, *15*, 303–312.

[99] L. Xing, K. Huang, S. Cao, H. Pang, *Chem. Eng. J.* **2018**, *332*, 253–259.

[100] K. Chen, X. Wang, W. Hu, Q. Kong, H. Pang, Q. Xu, *Small Struct.* **2022**, *3*, 2100200.

[101] N. Li, X. Guo, X. Tang, Y. Xing, H. Pang, *Chin. Chem. Lett.* **2022**, *33*, 462–465.

[102] F. Sun, Q. Li, Y. Bai, G. Zhang, S. Zheng, M. Peng, X. Chen, N. Lin, H. Pang, *Chin. Chem. Lett.* **2022**, *33*, 3249–3254.

[103] X. Chen, C. Wang, Y. Wang, J. Ma, Y. Dong, S. Gao, Q. Jing, W. Li, H. Pang, *J. Energy Storage* **2022**, *55*, 105319.

[104] Y. Zheng, S. Zheng, Y. Xu, H. Xue, C. Liu, H. Pang, *Chem. Eng. J.* **2019**, *373*, 1319–1328.

[105] J. Lu, H. Duan, Y. Zhang, G. Zhang, Z. Chen, Y. Song, R. Zhu, H. Pang, *ACS Appl. Mater. Interfaces* **2022**, *14*, 25878–25885.

[106] H. Duan, Z. Zhao, J. Lu, W. Hu, Y. Zhang, S. Li, M. Zhang, R. Zhu, H. Pang, *ACS Appl. Mater. Interfaces* **2021**, *13*, 33083–33090.

[107] H. Zhou, W. Cao, N. Sun, L. Jiang, Y. Liu, H. Pang, *Chin. Chem. Lett.* **2021**, *32*, 3123–3127.

[108] Y. Xu, Q. Li, H. Xue, H. Pang, *Coord. Chem. Rev.* **2018**, *376*, 292–318.

[109] S. Zheng, H. Xue, H. Pang, *Coord. Chem. Rev.* **2018**, *373*, 2–21.

[110] C. Liu, Y. Bai, W. Li, F. Yang, G. Zhang, H. Pang, *Angew. Chem. Int. Ed.* **2022**, *61*, e202116282.

[111] C. Liu, W. Feng, Y. Bai, H. Pang, *Inorg. Chem. Front.* **2022**, *9*, 5463–5468.

[112] Y. Bai, C. Liu, T. Chen, W. Li, S. Zheng, Y. Pi, Y. Luo, H. Pang, *Angew. Chem. Int. Ed.* **2021**, *60*, 25318–25322.

[113] S. Zheng, H. Zhou, H. Xue, P. Braunstein, H. Pang, *J. Colloid Interface Sci.* **2022**, *614*, 130–137.

[114] Q. Li, S. Zheng, Y. Xu, H. Xue, H. Pang, *Chem. Eng. J.* **2018**, *333*, 505–518.

[115] X. Jin, Y. Shan, F. Sun, H. Pang, *Trans. Tianjin Univ.* **2022**, *28*, 446–468.

[116] M. Yuan, X. Guo, N. Li, H. Pang, *J. Colloid Interface Sci.* **2021**, *589*, 56–64.

[117] Y. Li, Y. Xu, Y. Liu, H. Pang, *Small* **2019**, *15*, e1902463.

[118] S. Zheng, Y. Sun, H. Xue, P. Braunstein, W. Huang, H. Pang, *Natl. Sci. Rev.* **2022**, *9*, nwab197.

[119] G. Zhang, L. Jin, R. Zhang, Y. Bai, R. Zhu, H. Pang, *Coord. Chem. Rev.* **2021**, *439*, 213935.

[120] X. Hang, J. Zhao, Y. Xue, R. Yang, H. Pang, *J. Colloid Interface Sci.* **2022**, *628*, 389–396.

[121] Y. Li, Y. Shan, H. Pang, *Chin. Chem. Lett.* **2020**, *31*, 2280–2286.

[122] W. Yang, X. Shi, Y. Li, H. Pang, *J. Energy Storage* **2019**, *26*, 101018.